

UNIVERSITY OF MANCHESTER
SCHOOL OF MATERIALS

MICROWAVE DIELECTRIC CERAMICS

Supervisor-Prof. Freer

A dissertation submitted to University of Manchester for the
degree of Master of Science in the Faculty of Engineering and
Physical Sciences

2011

Yu-Cheng, Chiou

Declaration

No portion of the work referred to in the dissertation has been submitted in support of an application for another degree or qualification of this or any other university or institute of learning.

Abstract

Due to the telecommunication market expands and develops rapidly; both performance enhancement and lower price become main requirement of the microwave devices. $\text{Ba}_3\text{Co}_{0.7}\text{Zn}_{0.3}\text{Nb}_2\text{O}_9$ (BCZN) series dielectric ceramics with complex perovskite structure contain excellent dielectric properties, as well as low cost, but they are very sensitive to the process. Therefore, to investigate the factors impact to Qxf has been studied in this project. In this study, different heat treatment condition by controlling the sintering time, thickness and volume of BCZN systems are investigated. Previous study indicated ordering degree and domain size would influence Qxf value in perovskite structure system, therefore, the ordering parameter of B-site cation and domain size will obtain by the analysis of X-ray powder diffractiometer. Otherwise, the microstructure will be explored by SEM and optical microscopy.

The result show, Qxf value can be improved by increasing sintering time and reducing thickness. In this study, BCZN series microwave dielectric ceramics obtain the best Qxf value=99976 GHz when sample sintering at 1450°C for 4 hours and with 4.82 thickness.

Keyword: BCZN, dielectric, perovskite, B-site cation, ordering degree, domain size.

Acknowledgements

Many people have contributed to this Master degree. First, I would like to extend my sincere thanks to all the Professors and staffs in Manchester materials science school for teaching and giving assistance in the past year. In particular, I would like to say thanks for my supervisor, Prof. Freer, for his kindly and patiently pay attention for me, and help me through the whole course of this dissertation. And I also would like say thanks for Dr. Azough and Robert, for them assist me finish some complex experiment, as well as give suggestion of my project.

Secondly, I would say thanks for Ms. Judith Shackleton and Mr. Gary Harrison instruct me how to use XRD machine, and Mr. Michael Faulkner assist me to use SEM machine.

Thirdly, I also want to say thanks to my close friends who study in University of Manchester for giving me happiness and assistance in the past year. None of words can express my thankful feeling to all of them.

Finally, I would like say thanks for my parents for their support and encouragement.

SINCERE THANKS TO ALL

Table of contents

| | |
|--|-----|
| DECLARATION | I |
| ABSTRACT | II |
| ACKNOWLEDGMENTS | III |
| TABLE OF CONTENTS | IV |
| LIST OF TABLES | VI |
| LIST OF FIGURES | VII |
| | |
| <u>CHAPTER I - INTRODUCTION</u> | 1 |
| <u>CHAPTER II - BASIC THEORY AND LITERATURE REVIEW</u> | 3 |
| | |
| 2.1 Theory of microwave dielectric properties | 3 |
| 2.1.1 Dielectric constant | 3 |
| 2.1.2 Quality factor | 6 |
| 2.1.3 Temperature coefficient of resonant frequency | 7 |
| 2.2 Theory of microwave dielectric resonance | 8 |
| 2.3 Structure of complex perovskite ABO_3 system | 9 |
| 2.3.1 Tolerance factor | 10 |
| 2.4 Liquid phase sintering | 11 |
| 2.5 Microwave dielectric ceramics materials | 11 |
| 2.6 BZN, BCN and BCZN | 13 |
| 2.7 The factors affecting the quality factor | 14 |
| 2.7.1 Composition | 14 |
| 2.7.2 Processing conditions | 16 |
| 2.7.2.1 Cooling rate | 16 |
| 2.7.2.2 Anneal time | 16 |
| 2.7.2.3 Sintering temperature | 17 |
| 2.7.3 Additives | 19 |
| 2.7.4 Second phase | 20 |
| | |
| <u>CHAPTER III – EXPERIMENT PROCESSING AND ANALYSIS</u> | 23 |

METHODS

| | |
|--|----|
| 3.1 Preparation of materials | 23 |
| 3.2 Sepcimen analysis technique | 24 |
| 3.2.1 XRD | 24 |
| 3.2.2 Optical Microscopy | 27 |
| 3.2.3 Scanning Electron Microscopy (SEM) | 28 |

CHAPTER IV – RESULT AND DISCUSSION

| | |
|---|----|
| 4.1 The effect of thickness on the BCZN ceramics | 30 |
| 4.1.1 Phase analysis | 30 |
| 4.1.2 Microstructure analysis | 31 |
| 4.2 The effect of sintering time on the BCZN ceramics | 37 |
| 4.2.1 Phase analysis | 37 |
| 4.2.2 Microstructure analysis | 38 |
| 4.3 The effect of volume on the BCZN ceramics | 44 |
| 4.3.1 Phase analysis | 44 |
| 4.3.2 Microstructure analysis | 45 |
| 4.4 The effect of processing on the BCZN ceramics | 48 |
| 4.4.1 Phase analysis | 49 |
| 4.4.2 Microstructure analysis | 49 |
| 4.5 Overall discussion | 59 |
| 4.5.1 Comprehensive discussion of grain size | 59 |
| 4.5.2 Comprehensive discussion of Qxf value | 60 |
| 4.5.2.1 Secondary phase | 60 |
| 4.5.2.2 Ordering degree | 61 |
| 4.5.2.3 Domain size | 63 |

CHAPTER V – CONCLUSION AND FUTURE WORK

| | |
|-----------------|----|
| 5.1 Conclusion | 65 |
| 5.2 Limitation | 66 |
| 5.3 Future work | 66 |

REFERENCE

LIST OF TABLES

| | | |
|------------|--|----|
| Table 2.1: | Compositions, abbreviations, densities, and dielectric properties for the ceramics prepared. | 14 |
| Table 2.2: | Cooling rate VS dielectric properties (BZN). | 18 |
| Table 2.3: | Table 2.3 Cooling rate VS dielectric properties (BCN) . | 18 |
| Table 2.4: | Cooling rate VS dielectric properties (BCN). | 18 |
| Table 3.1: | Specimen in this project. | 23 |
| Table 3.2: | Operation condition in X'pert MPD diffractormeter . | 26 |
| Table 3.3: | Operation conditions in Philips X'pert-1. | 26 |
| Table 3.4: | SEM operation conditions. | 29 |
| Table 4.1: | Variation of ordering parameter. | 63 |
| Table 4.2: | Variation of domain size. | 64 |

LIST OF FIGURES

| | |
|---|----|
| Figure 2.1: Schematic representation of four mechanisms of polarization: | 5 |
| (a) electronic polarization, (b) ionic polarization, (c) orientation polarization, and (d) space charge polarization. | |
| Figure 2.2: Frequency dependence of several contributions to the polarization. | 6 |
| Figure 2.3: Transmission and reflection phenomenon at the interface. | 9 |
| Figure 2.4: The incident wave is guided in the medium as the totally internal reflection occurs. | 9 |
| Figure 2.5: Ideal cubic ABO_3 perovskite structure. | 11 |
| Figure 2.6: Dielectric properties vs composition for the $x\text{BZN}-(1-x)\text{BCN}$, 1987. | 15 |
| Figure 2.7: Dielectric properties vs composition for the $x\text{BZN}-(1-x)\text{BCN}$, 2003. | 16 |
| Figure 2.8: Dielectric properties vs composition for the $x\text{BNN}-(1-x)\text{BZN}$. | 17 |
| Figure 2.9: Variations of the relative density, the dielectric constant, the temperature coefficient of the resonant frequency and Q_{xf} value of BCN ceramics sintered at various temperatures for 6 h. | 19 |
| Figure 2.10: The density of BCZN with CeO_2 content vary. | 20 |
| Figure 2.11: The density of BCZN with V_2O_5 content vary. | 20 |
| Figure 2.12: Quality factor vs CeO_2 content in BCZN ceramics. | 21 |
| Figure 2.13: Quality factor vs V_2O_5 content in BCZN ceramics.. | 21 |
| Figure 3.1: X'pert MPD diffractometer. | 25 |
| Figure 3.2: Philips X'pert-1. | 26 |
| Figure 3.3: Selected areas for XRD selected areas for XRD. | 27 |
| Figure 3.4: Olympus BH2-OMA. | 28 |
| Figure 3.5: Selected areas for optical microscopy. | 28 |
| Figure 3.6: FESEM Philips XL30. | 29 |
| Figure 4.1: Q_{xf} value as a function of thickness. | 32 |
| Figure 4.2: XRD pattern of $\text{Ba}_3\text{Co}_{0.7}\text{Zn}_{0.3}\text{Nb}_2\text{O}_9$ series at various thicknesses. | 32 |

The samples were sintering at 1450°C for 4 hours.

| | |
|--|----|
| Figure 4.3: SEM photographs of specimens with different thicknesses sintered at 1450 °C/4 h. | 33 |
| Figure 4.4: Optical microscopy photographs of S1. | 34 |
| Figure 4.5: Optical microscopy photographs of S2. | 35 |
| Figure 4.6: Optical microscopy photographs of S3. | 36 |
| Figure 4.7: Grain size as a function of thickness. | 37 |
| Figure 4.8: Qxf value as a function of sintering time. | 38 |
| Figure 4.9: XRD pattern of $\text{Ba}_3\text{Co}_{0.7}\text{Zn}_{0.3}\text{Nb}_2\text{O}_9$ series at various sintering time. The samples were sintering at 1450°C. | 39 |
| Figure 4.10: photographs of specimens with different sintering time sintered at 1450 °C. | 40 |
| Figure 4.11: Optical microscopy photographs of S4. | 41 |
| Figure 4.12: Optical microscopy photographs of S5. | 42 |
| Figure 4.13: Optical microscopy photographs of S8. | 43 |
| Figure 4.14: Grain size as a function of sintering time . | 44 |
| Figure 4.15: Qxf value as a function of volume. | 45 |
| Figure 4.16: XRD pattern of $\text{Ba}_3\text{Co}_{0.7}\text{Zn}_{0.3}\text{Nb}_2\text{O}_9$ series at various volumes. The samples were sintering at 1450 for 16 hours. | 46 |
| Figure 4.17: Grain size as a function of to volume. | 46 |
| Figure 4.18: SEM photographs of specimens with different volumes sintered at 1450 °C/16 h. | 47 |
| Figure 4.19: Optical microscopy photographs of S6. | 48 |
| Figure 4.20: Qxf value. | 50 |
| Figure 4.21: XRD pattern $\text{Ba}_3\text{Co}_{0.7}\text{Zn}_{0.3}\text{Nb}_2\text{O}_9$ series at various compositions. The samples were sintering at 1450°C for 24 hours. | 51 |
| Figure 4.22: XRD pattern of $\text{Ba}_3\text{Co}_{0.7}\text{Zn}_{0.3}\text{Nb}_2\text{O}_9$ series at various compositions. The samples were sintering at 1450°C for 24 h. | 52 |
| Figure 4.23: XRD pattern of $\text{Ba}_3\text{Co}_{0.7}\text{Zn}_{0.3}\text{Nb}_2\text{O}_9$ series at various compositions. The samples were sintering at 1450°C for 24 h. | 53 |
| Figure 4.24: XRD pattern of $\text{Ba}_3\text{Co}_{0.7}\text{Zn}_{0.3}\text{Nb}_2\text{O}_9$ series at various time, all sample sintering at 1450°C. | 54 |

| | |
|---|----|
| Figure 4.25: SEM photographs of specimens with different composition sintered at 1450 °C/4 h. | 55 |
| Figure 4.26: SEM photographs of specimens with different composition sintered at 1450 °C/16 h. | 56 |
| Figure 4.27: SEM photographs of specimens with different composition sintered at 1450 °C/24 h. | 57 |
| Figure 4.28: SEM photographs of specimens sintering at 1450 °C/4 h closed to surface phase. | 58 |
| Figure 4.29: SEM photographs of specimens sintering at 1450 °C/4 h closed to matrix phase. | 58 |
| Figure 4.30: Optical microscopy photographs of S10. | 59 |

Chapter I

INTRODUCTION AND AIM

When electromagnetic waves pass through dielectric materials, a standing wave is generated in the dielectric body due to the strengthening of interference on reflection wave and incident wave form on the interface between air and material internal, this phenomenon called “resonance”. The dielectric resonators are produced by this phenomenon. The term initial appeared in 1939 in Richthmyer [1] paper, he try to figure out whether the ring dielectric materials can be used as dielectric resonator, 1960s, people began to study the microwave frequency range of dielectric materials, and applied to microwave filter.

Recently, due to the greatly growth of commercial wireless technologies such as mobile phone, global positioning systems, as well as in satellite broadcasting systems, it is very important to design high quality devices to increase the performance of mobile communication systems. In the application field of microwave dielectrics, materials not only need as small as possible, but also to be required excellent in three dielectric properties [2]. Firstly, dielectric constant (ϵ_r) need as large as possible in order to get small size, because the size of a resonator is inversely proportional to the square root of relative permittivity. Secondly, high Q value ($1/\tan\delta$) is necessary to attain high frequency selectivity and stability in microwave transmitter and recipient components. Thirdly, temperature coefficient of the resonant frequency (τ_f) is required to be as close to 0 ppm/ $^{\circ}\text{C}$ as possible, it can make sure the signal is stable during devices operation. With these characteristics, dielectric resonators are investigated and widely used in as components of microwave filters and oscillators. In order to achieve these materials targets, developing and researching of new materials has become more important. Ceramic materials have a notable advantage in reducing size and superb characteristics in dielectric property; therefore, there were many studies of ceramic dielectric resonator since the 1960s [3]. Moreover, there was a breakthrough in dielectric properties after 1981, especially in quality factor.

However, most early ceramics dielectric resonators were based on TiO_2 [4] or Ta_2O_5 [5], and there were some problems requiring improvement. Firstly, temperature coefficient of resonant frequency for TiO_2 is too large for practical applications, and the price of Ta_2O_5 increased to more than \$350/kg [2]. Hence, scientist and engineer try to investigate new materials which have excellent dielectric properties and low price. For these reason, Na_2O_5 -based ceramic dielectric resonators emerged and were employed in commercial industry due to their lower price. Previous literature has indicated that the Na_2O_5 -based dielectric resonators which are formed in the perovskite structure have good dielectric properties; these include materials such as $\text{BaCo}_{1/3}\text{Nb}_{2/3}\text{O}_3$ (BCN) and $\text{BaZn}_{1/3}\text{Nb}_{2/3}\text{O}_3$ (BZN).

Although $\text{BaZn}_{1/3}\text{Nb}_{2/3}\text{O}_3$ has good dielectric constant (ϵ_r) and high quality factor, the temperature coefficient of the resonant frequency (τ_f) is too high. In order to reduce the temperature coefficient of the resonant frequency (τ_f) to zero, addition of 40%[2] $\text{BaCo}_{1/3}\text{Nb}_{2/3}\text{O}_3$ doped could reach this goal. Therefore the $\text{Ba}(\text{Co}_{0.7}\text{Zn}_{0.3})_{1/3}\text{Nb}_{2/3}\text{O}_3$ (BCZN) which has complex perovskite structure emerged.

Since the properties of ceramics dielectric resonators are very sensitive to processing conditions, then the aim of this study is to investigate the main factors influencing the properties of $\text{Ba}(\text{Co}_{0.7}\text{Zn}_{0.3})_{1/3}\text{Nb}_{2/3}\text{O}_3$ (BCZN) dielectric properties. This will address, for example, the ordering degree in different parts of the sample surface phase, sintering schedule, microstructure and doping.

CHAPTER II

BASIC THEORY AND LITERATURE REVIEW

2.1 Theory of microwave dielectric properties

Since the 1980s, more and more researchers have investigated the development of ceramic dielectric material; therefore, there is better dielectric resonator materials have appeared. Ceramic resonators, instead of traditional metal cavity resonators, became the trend due to good dielectric properties. An ideal ceramic microwave dielectric resonator must have the following three characteristics [6]:

- A. Dielectric constant (ϵ_r): In the microwave frequency band, typically $20 < \epsilon_r < 100$. Dielectric constant influences the dielectric resonator size. (ϵ_r value higher, dimensions can be smaller).
- B. Dielectric quality factor (Q): The reciprocal of the dielectric loss ($\tan\delta$). Q-value directly affects the energy loss when the resonator is used. The greater the Q value, then smaller the signal loss.
- C. Temperature coefficient of resonant frequency (τ_f): General requirements are between $-5 \text{ ppm} / {}^\circ\text{C} < \tau_f < +5 \text{ ppm} / {}^\circ\text{C}$. Temperature coefficient of resonant frequency should be small to ensure the stability of operating frequency in order to avoid drift when temperature changed.

The following sections will describe the theory and detail of those three dielectric properties respectively.

2.1.1 Dielectric constant

For dielectric materials, the dielectric constant is mainly determined by its ability to be polarized. The phenomenon of polarization is due to external electric field applied to a dielectric material, the atomic or molecular dipoles are aligned. According to the explanation above, the dielectric properties of microwave dielectric materials result

from polarization phenomenon and the relationship between electric polarization and dielectric constant can be expressed as in equation (2-1):

$$\begin{aligned} P &= \epsilon_0 (\epsilon_r - 1) E \\ \epsilon_r &= \frac{\epsilon}{\epsilon_0} \end{aligned} \quad (2-1)$$

In which

P : is the electric polarization.

E : is the external electric field.

ϵ : is the relative permittivity

ϵ_0 : is the permittivity of free space.

Fig 2-1 and fig. 2-2 show, the polarization mechanism can be divided into four types with different frequencies [7].

- A. Electronic polarization: The phenomenon occurs in all materials, the atomic electron cloud biased at one end due to an applied electric field. The frequency range is greater than 10^{14} Hz.
- B. Ionic polarization: Cation and anion are migration in the ion crystal due to mutual attraction. The frequency range is around $10^{10} \sim 10^{14}$ Hz.
- C. Orientation polarization: Polar molecules are being influenced by the applied electric field, the direction of electric dipole arrange parallel to electric field. The frequency range is about $10^4 \sim 10^{10}$ Hz.
- D. Space charge polarization: Removable charge gathered at the interface (grain boundary, phase boundary) and arranged with the electric field direction due to external electric field. The frequency range less than 10^3 Hz.

The equation (2-2) shows as below explains the Microwave wavelength in the medium:

$$\lambda_g = \frac{\lambda_0}{\sqrt{\epsilon_r}} \quad (2-2)$$

Where

λ_g : is the wavelength in the medium.

λ_0 : is the wavelength in the free space.

ϵ_r : Really relative permittivity.

The equation clearly point out that the sizes of dielectric resonators can be reduced as the dielectric constant goes up. Therefore, component size can be minimized.

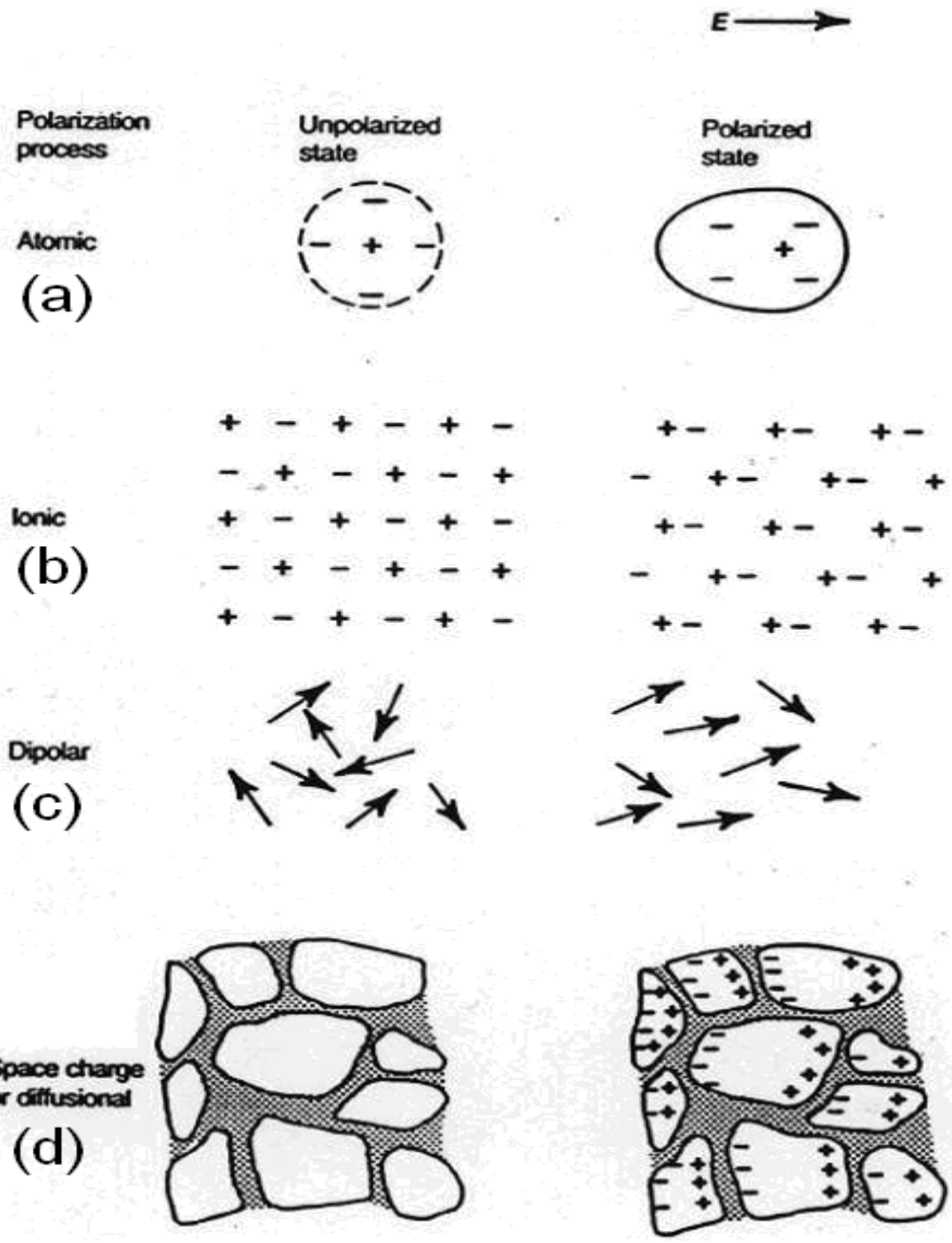


Fig. 2-1 Schematic representation of four mechanisms of polarization: (a) electronic polarization, (b) ionic polarization, (c) orientation polarization, and (d) space charge polarization. (Take from Kingery et al [8])

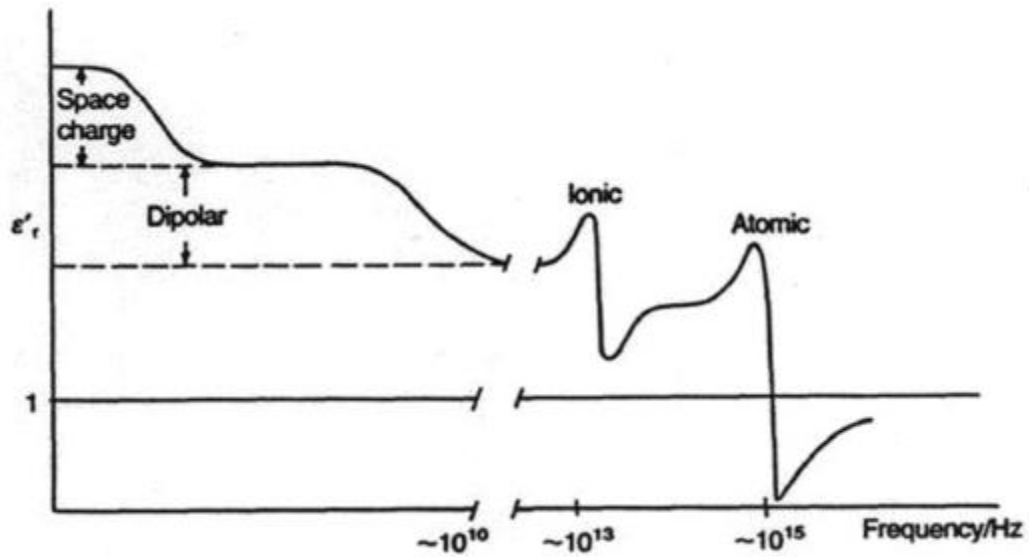


Fig. 2-2 Frequency dependence of several contributions to the polarization. (Take from Kingery et al [8])

2.1.2 Quality factor [9]

The definition of the Quality factor can be expounded as shown in equation (2-3):

$$Q = \frac{2\pi W_0}{PT} = \frac{\omega_0 W_0}{P} \quad (2-3)$$

Where:

W_0 : Stored energy.

P : Power consumption.

ω_0 : Microwave frequency.

T : period.

The equation indicates that the quality factor is direct proportional to the stored energy; on the other hand it has an inverse ratio to the power consumption. It means greater quality factor leads to smaller consumption of power.

Meanwhile, the frequency bandwidth of a resonator and the Q value are inversely proportional (Shown as equation 2-4), so that high Q value resonator has narrow bandwidth.

$$Q = \frac{f_0}{f_2 - f_1} \quad (2-4)$$

Where:

f_0 : Resonance frequency.

$f_2 - f_1$: - 3 dB bandwidth.

There are several different Q values that need to consider when the dielectric resonator is applied as the microwave circuit load [10]: namely the unloaded Q-factor (Q_0) which is affected by internal dielectric resonance: external Q-factor (Q_E) which is influenced by external electric circuitry loss: loaded Q-factor (Q_L) which includes internal and external loss.

Generally, when measured and compared the Q value of the same dielectric resonator specimen, would vary due to size of sample. Typically, the variation of the Q value multiplied by resonant frequency is very small for 1 to 20 GHz, it can be regarded as a constant value [11]. Thus, Q value is often expressed as $Q \times f$ (GHz) to represent, which can easily compare Q-values.

The factors influencing the Q-value under microwave frequency are described as follow [12]:

- A. Internal loss: A the homogeneous crystalline material, due to a number of point defects or dopant atoms, leading to scattering, and then resulting in damping.
- B. External loss: In inhomogeneous materials, due to dislocations, grain boundaries, impurities and second phases leading to loss, mainly related to the material processing.

2.1.3 Temperature coefficient of resonant frequency [10]

Temperature coefficient of resonant frequency is defined as the resonant frequency sensitivity to temperature changes, units ppm / °C. As the resonance frequency f_0 varies with dielectric constant and size of specimen, the relationship can be expressed as equation (2-5):

$$f = \frac{C}{D\epsilon^{1/2}} \quad (2-5)$$

Moreover, the relation between the temperature and D and ϵ can be explained as the equation (2-6) which is the derivative with respect to temperature from equation (2-5).

$$\frac{1}{f} \frac{\partial f}{\partial T} = \frac{-1}{D} \frac{\partial D}{\partial T} - \frac{1}{2\epsilon} \frac{\partial \epsilon}{\partial T} \quad (2-6)$$

Where

$\tau_f = \frac{\partial f}{\partial T}$: Temperature coefficient of resonant frequency

$\alpha = \frac{1}{D} \frac{\partial D}{\partial T}$: Linear thermal expansion coefficient of materials

$$\tau\epsilon = \frac{1}{\epsilon} \frac{\partial \epsilon}{\partial T}$$

Temperature coefficient of dielectric constant

Thus, equation 2-6 can be rewritten as equation (2-7):

$$\tau_f = -\alpha - \frac{1}{2} \tau\epsilon \quad (2-7)$$

According to equation (2-7), in order to achieve $\tau_f=0$, α should be equal to $-\frac{1}{2}\tau\epsilon$.

Otherwise, most materials have positive thermal expansion coefficient, so a negative temperature coefficient of dielectric constant is necessary.

2.2 Theory of microwave dielectric resonance

According to classical electromagnetic theory explain: when an incident electromagnetic wave passes through a dielectric material, part will be reflected beams and part of transmitted (Fig. 2-3) due to the dielectric permittivity of the materials being larger than the air. Thus, the electromagnetic energy which incident on the dielectric material will be closed inside to form a standing wave (shown as Fig. 2-4). This phenomenon is known as “dielectric resonance” [13]. According to Snell’s law [14], the equation (2-8):

$$\frac{\sin\theta_t}{\sin\theta_i} = \frac{n_1}{n_2} = \frac{\sqrt{\epsilon_1}}{\sqrt{\epsilon_2}} \quad (2-8)$$

If the wave is obliquely incident, the reflected wave obeys Snell’s law of reflection, which says that the reflection angle is equal to the incident angle. Moreover, the transmitted wave also obeys Snell’s law of refraction and states that the ratio between incident angle and transmit angle is inverse ratio of indices of refraction n_1/n_2 .

In addition, according to the Snell’s law, the critical incident angle can be derived as $\sin^{-1}(\frac{\sqrt{\epsilon_1}}{\sqrt{\epsilon_2}})$ [14]. If the incident angle is greater than the critical incident angle, total internal reflection occurs. It means that the ϵ_r needs to increase with incident angle increase, if desired total internal reflection occurs. In the practice case, whenever ϵ_r is bigger than 2, total reflection obtained and the energy is closed inside the material due to $\epsilon_r \geq 1 + \sin^2\theta_i$ (the dielectric constant in air is 1 and $\sin^2\theta_i \leq 1$).

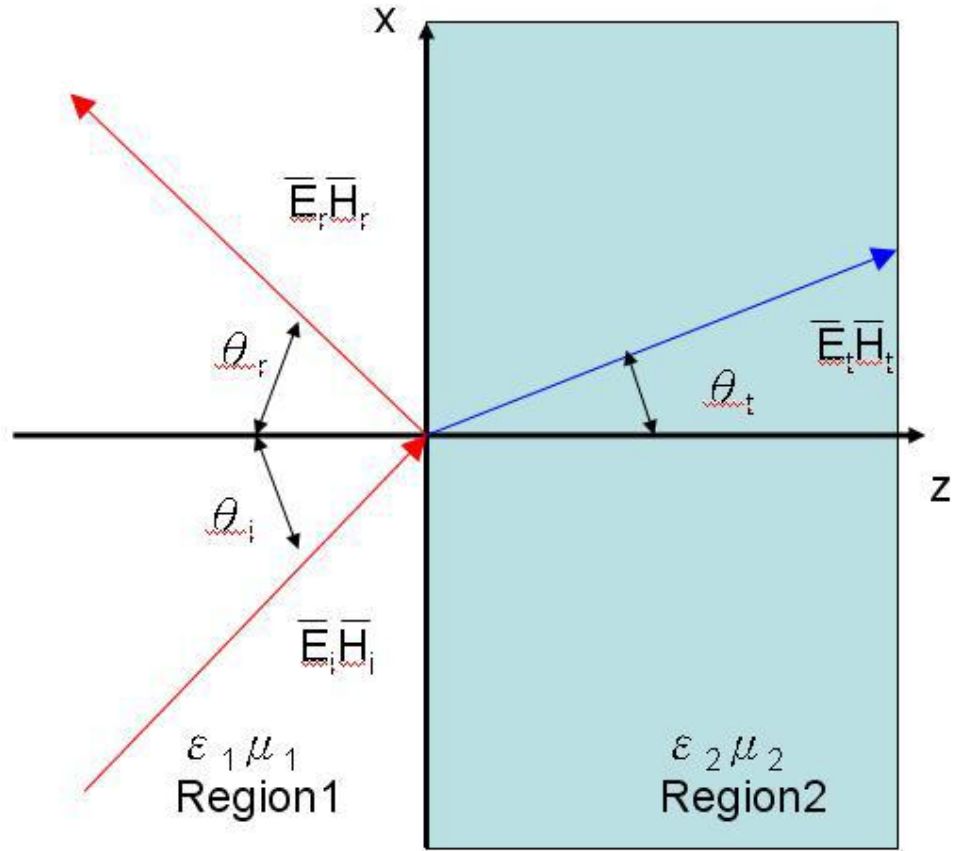


Fig. 2-3: Transmission and reflection phenomenon at the interface. (Take from cheng [14])

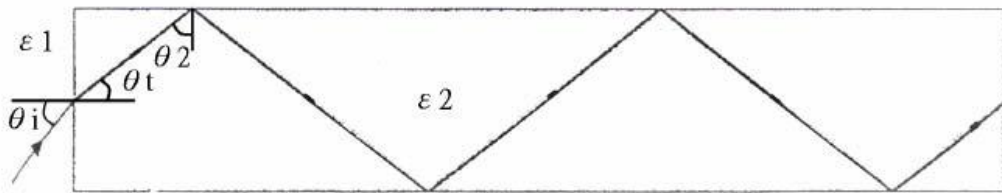


Fig. 2-4: The incident wave is guided in the medium as the totally internal reflection occurs. (Take from cheng [14])

2.3 Structure of complex perovskite ABO_3 system

The perovskite structure (Fig. 2-5) is found in any material with the same type of crystal structure [15], known as the perovskite structure. It is a ternary compound of formula ABO_3 that A and B cations differ in size. It is considered an FCC- derivative structure in which the larger A cation and oxygen together form an FCC lattice while the smaller B cation occupies the octahedral interstitial sites in the FCC array. There is only the

oxygen being B cation's nearest neighbor.

Perovskite structure types can be described base on B-site ordering. There are three main types in perovskite structures [16]; (i)1:1 ordering $A(B'_{1/2}B''_{1/2})O_3$; (ii)1:2 ordering $A(B'_{1/3}B''_{2/3})O_3$ (iii)1:3 ordering $A(B'_{1/4}B''_{3/4})O_3$. With an ordering change, it might form different structure, for example, 1:1 ordering usually with cubic and 1:2 ordering forms as part cubic and part of hexagonal or pure hexagonal.

Altering the degree of order can induce substantial changes in magnetic behavior, dielectric or ferroelectric response, and electronic or ionic conductivity. Therefore, perovskite structure materials may be a high priority in commercial microwave communication devices. Recently, Nb_2O_5 -based or Ta_2O_5 -based materials with 1:2 ordering on B-site exhibit very low dielectric losses.

2.3.1 Tolerance factor

The tolerance factor proposed by Goldschmidt [17] can be used to define the nature of the perovskite structure by the relationship between the radii of each ionic species.

The relationship between tolerance factor and ionic radius is shown as equation 2-9:

$$t = \frac{rA+rO}{\sqrt{2}(rB+rO)} \quad (2-9)$$

For the perovskites structure, it must meet the following conditions [17]:

- A. Tolerance factor must be around $0.77 < t < 1.1$, if a stable perovskites structure desired. If $t < 0.75$, the structure may be formed ilmenite; if $t > 1.1$, it may form calcite, aragonite structure.
- B. The cations in the A-site or B-site must be able to stabilize in their own environment.
- C. The radii of cations in A-site and B-site are $rA > 0.90 \text{ \AA}$, $rB > 0.51 \text{ \AA}$ respectively.

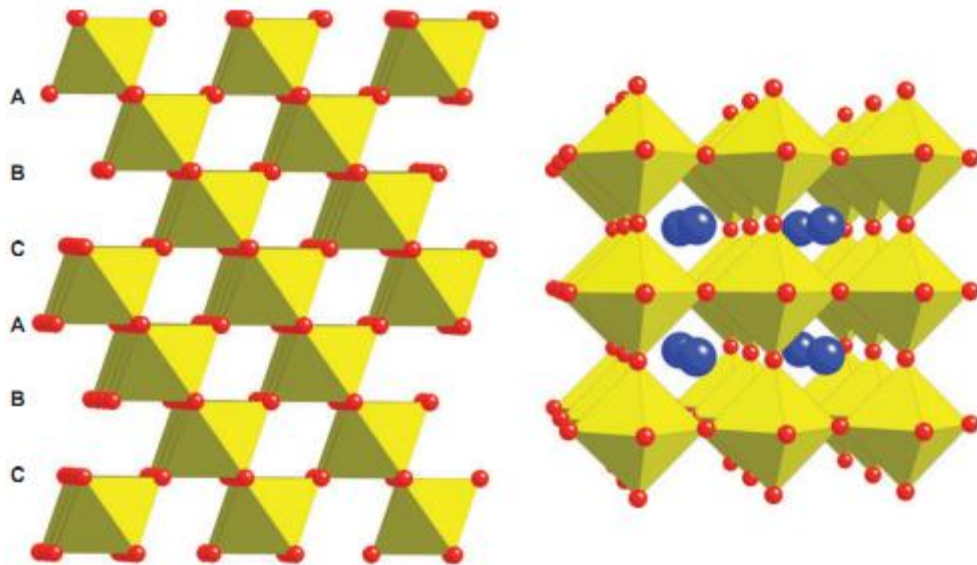


Fig 2.5 Ideal cubic ABO_3 perovskite structure. (Take from Davies et al [16])

2.4 Liquid Phase Sintering [18, 19]

The definition of liquid phase sintering is: during the thermal cycle, sintering involves a coexisting of liquid and particulate solid. Faster sintering and lower sintering temperature are the main advantages of liquid sintering. In the ceramic sintering process, the dielectric resonator can produce a higher density due to material appears liquid-phase sintering. Therefore, this section will be explored liquid sintering. According to Kingery [20] research shown liquid-phase sintering can be divided into three stages:

- A. Rearrangement Process
- B. Solution-Precipitation Process
- C. Coalescence Process

In addition, in order to achieve the success of the liquid-phase sintering, must meet the following three conditions [21]: 1.the appropriate amount of liquid; 2.solid need has appropriation solubility to liquid; 3.solid must be completely wet by liquid.

2.5 Microwave dielectric ceramics materials

In the microwave dielectric ceramics field, the earliest research could be tracked back to 1960s when they were applied as dielectric filters. Until now, there are several kinds

of materials have been developed and can be broadly divided into five types by composition and structure.

A. (Ca, Sr, Ba) ZrO₃ system:

These kinds of materials are based on three zirconate materials CaZrO₃, SrZrO₃ and BaZrO₃, and they are amongst the first dielectric materials [22]. With the amount of Ca, Sr and Ba vary; the microwave dielectric properties would be changed [23]. However, ϵ_r and Q value in this system are lower. Yamaguchi et al [23] shown that: Q value around 2000~3000 at 11 Ghz, relative permittivity about 29~32 and temperature coefficient of dielectric constant about -50 to +50 ppm/°C

B. ZrO₂-SnO-TiO system:

Zirconate titanium (Zircornium Titanate, ZrTiO₄) series has been used as dielectric materials due to temperature stable. With add Sn can obtain a high Q value and low temperature coefficient of resonant frequency material which is suitable for dielectric resonance materials [24]. In addition, the dielectric properties of this system depend on its composition, additives and sintering conditions [25]. Osband et al [24] show that this series material can achieve: (i) a permittivity greater than 35, (ii) a dielectric Q greater than 5×10^3 at 6 GHz and (iii) a temperature coefficient of permittivity close to zero

C. BaO-PbO-Nd₂O₃-TiO₂ system:

These materials are with higher dielectric constant about 90 [26], but the quality factor is lower. Wakino [26] et al shown that (Zr, Sn)TiO₄ has a higher relative permittivity=38, Q value= 7000 at 7 GHz and temperature coefficient of resonant frequency τ_f = 0 ppm/°C.

D. BaO-TiO₂ system:

This material system used in the microwave range usually with high TiO₂ content. However, there is only few materials stable, such as Ba₆Ti₁₇O₄₀、Ba₄Ti₁₃O₃₀、BaTi₄O₉ and Ba₂Ti₉O₂₀ [27]. Due to the temperature stable, even BaTi₄O₉ contain the maximum Q value, but if taking into account the temperature coefficient, Ba₂Ti₉O₂₀ which with lower Q value and temperature coefficient is better [28], in which the relative permittivity = 39.8, Q value= 8000

at 4 GHz, and τ_f (temperature coefficient of dielectric constant) = -24 \pm 2 ppm/ $^{\circ}$ C

E. Complex perovskites A (b' _{1/3} B'' _{2/3})O₃ structure system:

Recently, Complex perovskites structure dielectric resonators are high demand material, engineer prefer use this structure materials due to its high Q value.

For example Ta₂O₅-based materials, such as Ba (Zn_{1/3}Ta_{2/3})O₃ (BZT) and Ba (Mg_{1/3}Ta_{2/3})O₃ (BMT) have high Q_{xf0} value about 250,000–300,000 GHz [6], as well the dielectric constant increase without Q value decrease by doped [29]

However, with the Ta₂O₅ price increase and mobile telephone market increase, low cost materials would be considered. Therefore, Nb₂O₅-based ceramic dielectric resonators which are with complex perovskites structure are investigated [2], such as Ba(Zn_{1/3}Nb_{2/3})O₃ (BZN) [30] and Ba(Co_{1/3}Nb_{2/3})O₃ (BCN) [31] as well as Ba₃Co_{0.7}Zn_{0.3}Nb₂O₉ (BCZN) [2] which is made from Ba(Zn_{1/3}Nb_{2/3})O₃ (BZN).

2.6 BZN, BCN and BCZN

Since the price of Ta₂O₅ has increased to more than \$350/kg [2], the Nb₂O₅ which at a low cost around \$40/kg [2] gradually become based materials to dielectric resonator ceramic and more and more study in this system. This study will focus on Ba (Co, Zn)NbO₃ series materials, and the dielectric properties and structure are briefly introduce as below:

- A. Ba(Zn_{1/3}Nb_{2/3})O₃: BZN which with perovskite structure has a dielectric constant of 40, a quality factor greater than 60,000 GHz and a positive temperature coefficient of resonant frequency about +20ppm / $^{\circ}$ C [32]. Ignoring the problem of temperature coefficient of resonant frequency, BZN still has potential to be used as a microwave dielectric ceramic [2].
- B. Ba(Co_{1/3}Nb_{2/3})O₃: BCN formed as in either a disordered cubic or in an ordered hexagonal perovskite structure, and having a dielectric constant around 32.5, a quality factor about 60000 GHz and negative temperature coefficient of resonant frequency about -10ppm / $^{\circ}$ C [32].
- C. Ba₃Co_{0.7}Zn_{0.3}Nb₂O₉: In order to reach temperature coefficient of resonant

frequency close to 0, researchers made a module based on the formulation $x\text{BZN} + (1 - x)\text{BCN}$ [32] to try to achieve this goal. Hughes et al [2] pointed out that 40% Zn substitution to Co could result in zero temperature coefficient of resonant frequency. Therefore, BCZN microwave dielectric ceramics have been developed. According to Hugh et et al [2] study, BCZN series microwave dielectric ceramic $0.9\text{BCZN}+0.1\text{BGT}$ has a Q value=32 000 at 3.05 GHz, relative permittivity =35, and $\tau_f=0$.

Table 2.1: Compositions, abbreviations, densities, and dielectric properties for the ceramics prepared.
(Take from Hughes et al [2])

| Composition | Abb. | Density (g cm ⁻³) | ϵ_r | ϱ | f_0 (GHz) | τ_f (ppm/°C) |
|---|---------------------|----------------------------------|--------------|-----------|-------------|----------------------|
| $\text{Ba}(\text{Zn}_{0.33}\text{Nb}_{0.67})\text{O}_3$ | BZN | 6.4 | 39 | 17 100 | 2.848 | 28 |
| $0.95\text{Ba}(\text{Zn}_{0.33}\text{Nb}_{0.67})\text{O}_3$ – $0.05\text{Ba}(\text{Ga}_{0.5}\text{Ta}_{0.5})\text{O}_3$ | 0.95BZN- 0.05BGT | 6.4 | 38 | 34 900 | 2.949 | 19 |
| $0.9\text{Ba}(\text{Zn}_{0.33}\text{Nb}_{0.67})\text{O}_3$ – $0.1\text{Ba}(\text{Ga}_{0.5}\text{Ta}_{0.5})\text{O}_3$ | 0.9BZN- 0.1BGT | 6.4 | 37 | 31 600 | 2.963 | 15 |
| $0.9\text{Ba}([\text{Zn}_{0.60}\text{Co}_{0.40}]_{0.33}\text{Nb}_{0.67})\text{O}_3$ – $0.1\text{Ba}(\text{Ga}_{0.5}\text{Ta}_{0.5})\text{O}_3$ | 0.9BCZN- 0.1BGT | 6.5 | 35 | 32 000 | 3.056 | 0 |

2.7 The factors affecting the quality factor

In the field of dielectric filter application, the size is not as important as dielectric oscillators, therefore the dielectric constant only needs to be enough for total internal reflection to occur. So, the most important requirement would be quality factor which should be as large as possible to ensure maximum signal discrimination [6]. As the dielectric properties would be influenced by manufacturing processes and conditions there has been much work to identify the factors influencing the quality factor as well as how to improve it to maximum.

2.7.1 Composition

Adjusting the composition of material is not only to achieve temperature coefficient of resonant frequency close to zero, but also to reach optimized quality factor. Ando et al [33] summarized the dielectric properties compare with the $x\text{BZN}-(1 - x)\text{BCN}$ system (in which x from 0.1 to 0.9) results are shown as Fig 2.5 [33]. This study indicated the

quality factor would be decreased from 13000 to 100000 GHz as the BZN content increased, temperature coefficient of resonant frequency could be close to zero when $x=0.3$, and dielectric constant could achieve the maximum around 39 at $x=0.9$. In 2003, Ahn et al [32] built similar experiment with the same system and also confirmed the trend of dielectric properties when BZN content increase (Fig 2.6).

Moreover, for ceramics in the system $\text{Ba}(\text{Zn}_{1/3}\text{Nb}_{1/2})\text{O}_3-\text{Ba}(\text{Ga}_{1/2}\text{Ta}_{1/2})\text{O}_3$ (BZN-BGT), the quality factor goes up with BGT added and can achieve maximum in 0.95BZN-0.05BGT system about 34900 at 2.949 GHz. Temperature coefficient of resonant frequency can be reduced to 15 ppm / °C with 10% BGT added.

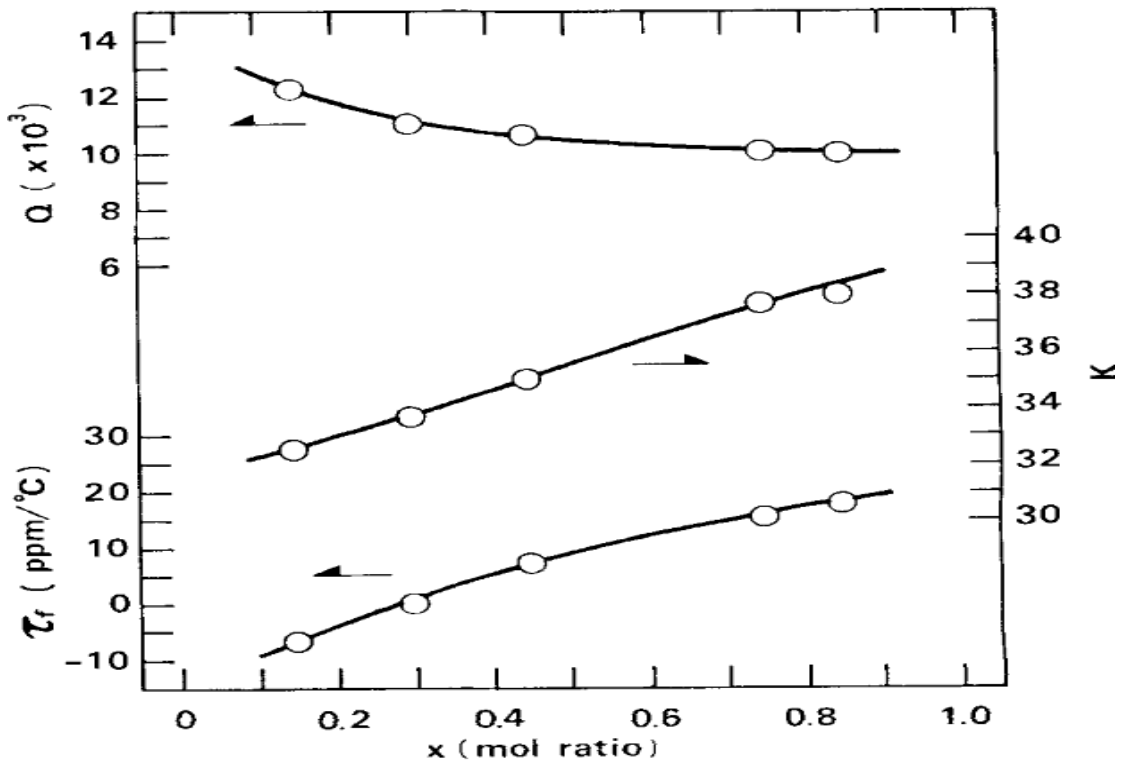


Fig. 2.6: Dielectric properties vs composition for the $x\text{BZN}-(1-x)\text{BCN}$, 1987. (Take from ANDO et al [33]).

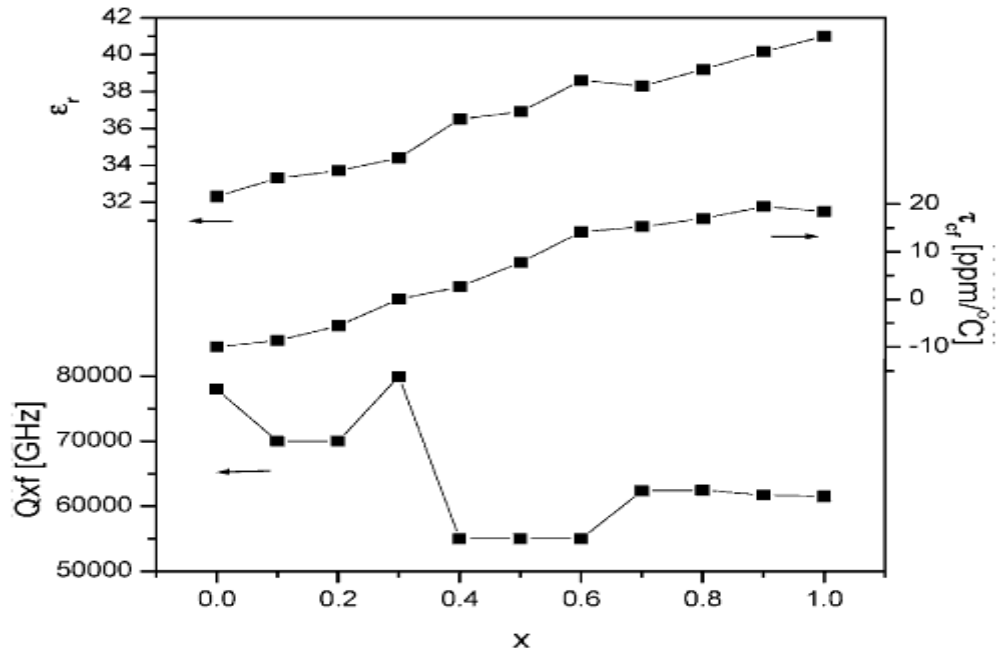


Fig. 2.7: Dielectric properties vs composition for the $x\text{BZN}-(1-x)\text{BCN}$, 2003. (Take from Ahn et al [32])

2.7.2 Processing conditions

Generally speaking, the material production processes include milling, drying and calcining, sintering, cooling and annealing. As the dielectric ceramics are very sensitive to the process conditions, the production processes have an influence on quality factor.

2.7.2.1 Cooling Rate:

Cooling rate would influence the grain size, the density of domains [6], and B-site cation ordering in the perovskite structure [34]. Tables 2.2, 2.3 and 2.4 [34] illustrate the quality factor would increase with a slower cooling rate in Nb-based microwave dielectric ceramics. Slower cooling can reduce the density of domains and lead to B-site cation ordering 1:2, therefore the quality factor increase [6, 34, 35].

2.7.2.2 Anneal time:

Barwick et al [36] showed that the amount of x from 0.2 to 0.9 has very low quality factor in $x\text{BZN}-(1-x)\text{BCN}$ ceramics system. The original quality factor is 25000 and 50000 GHz (2-8-6) in BZN and BNN, respectively, but the quality factors are less than

10000 from $x=0.2$ to $x=0.9$. The authors indicated that $0.35(\text{Ba}(\text{Ni}_{1/3}\text{Nb}_{2/3})\text{O}_3)-0.65(\text{Ba}(\text{Zn}_{1/3}\text{Nb}_{2/3})\text{O}_3$ which has Q value lower than 5000 GHz demonstrate good quality factor about 25000 GHz after sintering at 1450°C for 4 h and annealing at 1300°C for 72 h [36]. The main effect of annealing is to increase homogeneity. Therefore, there is less internal loss.

2.7.2.3 Sintering temperature:

When elements evaporate or phases melt, the composition would be changed in the liquid phase. Therefore, controlling the sintering temperature becomes a challenge, because the dielectric properties might change. Fig. 2.8 [33] shows the relationship between the dielectric properties and sintering temperature in BCN ceramics. Except for quality factor, all vary in a reasonable range. The quality factor reaches maximum about 78000 Ghz for 1400°C , and declines dramatically from 1400°C to 1500°C and being close to zero after sintering at 1550°C . Ahn et al [33] suggested the trend was due to the presence of resulting liquid phase.

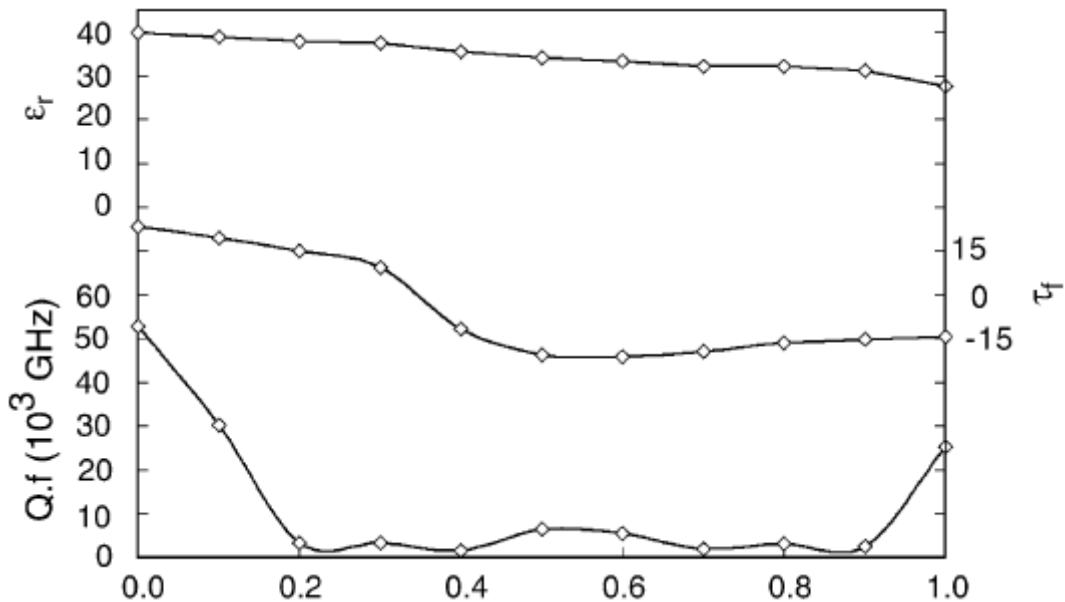


Fig. 2.8 Dielectric properties vs composition for the $x\text{BNN}-(1-x)\text{BN}$ (2-8-6, take from Barwick et al)

Table 2.2 Cooling rate VS dielectric properties (BZN) (2-8-8 take from Azough et al)

| | | | |
|---------------------------|-------|-------|-------|
| Cooling rate [°C/hour] | 360 | 60 | 5 |
| Quality factor [GHz] | 32000 | 56000 | 98000 |
| ϵ_r | 40 | 39.6 | 39.4 |
| τ_f [ppm/°C] | 23 | 22 | 21 |

Table 2.3 Cooling rate VS dielectric properties (BCN) (2-8-8, take from Azough et al)

| | | | |
|------------------------|-------|-------|-------|
| Cooling rate [°C/hour] | 360 | 60 | 5 |
| Quality factor [GHz] | 22000 | 41000 | 66500 |
| ϵ_r | 32.4 | 32.2 | 32 |
| τ_f [ppm/°C] | -14 | -12 | -10 |

Table 2.4 Cooling rate VS dielectric properties (BCN) (2-8-8, take from Azough et al)

| | | | |
|------------------------|-------|-------|-------|
| Cooling rate [°C/hour] | 360 | 60 | 5 |
| Quality factor [GHz] | 10000 | 20000 | 28000 |
| ϵ_r | 31.8 | 31.6 | 31 |
| τ_f [ppm/°C] | | | -18 |

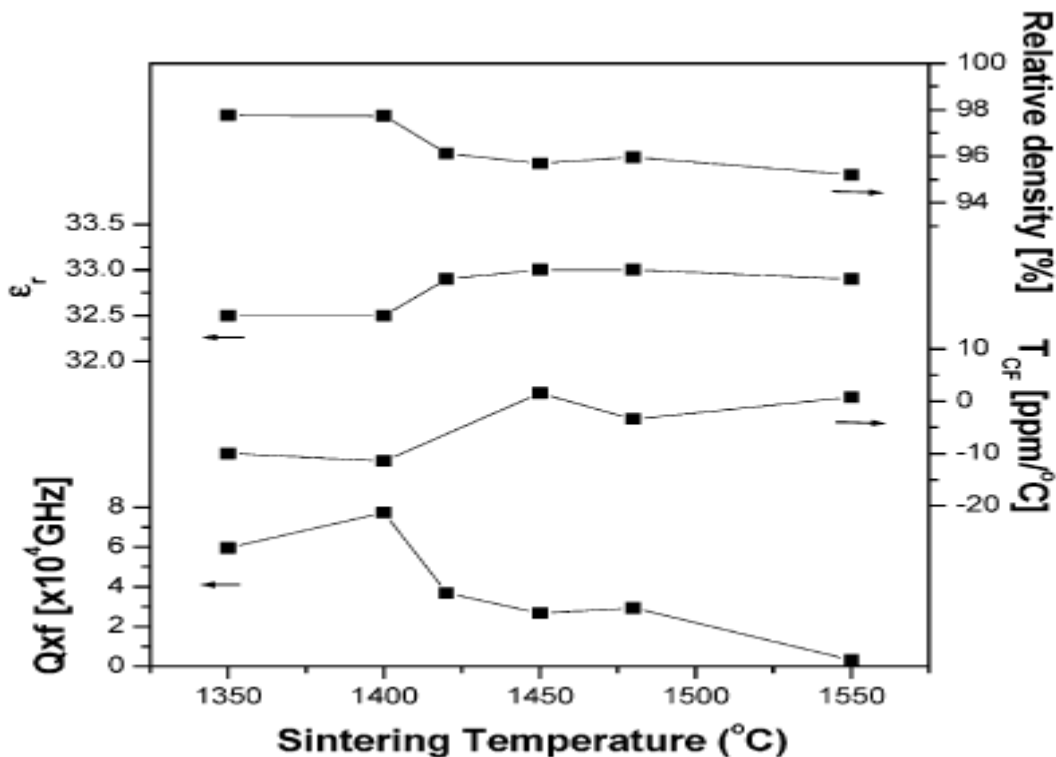


Fig. 2.9 Variations of the relative density, the dielectric constant, the temperature coefficient of the resonant frequency and Q_{rf} value of BCN ceramics sintered at various temperatures for 6 h (Take from ahn et al [33])

2.7.3 Additives

In dielectric ceramic materials, additives are the most effective way to increase the density. Fig 2.9 and 2.10 confirmed that the additives used by Azough et al [35, 36] have a positive impact on the density in BCZN ceramics. The undoped BCZN only was 70% theoretical after sintering at 1450°C. However, with additives, the density achieved 95% theoretical. Fig. 2.11 and Fig 2.12 show the quality factor against to additives, with the information from Fig 2.9 and 2.10, F. Azough et al [35, 36] suggest the quality factor would increase with density. The results illustrated BCZN ceramics can reach maximum quality factor around 84000 GHz with 0.4wt% CeO₂ added, a sintered at 1450°C for 4h and cooled at 60 °C/h [35] and 8500 GHz with 0.025 wt.% V₂O₅ addition sintered at 1450°C for 4h and annealed in nitrogen atmosphere for 4h [36].

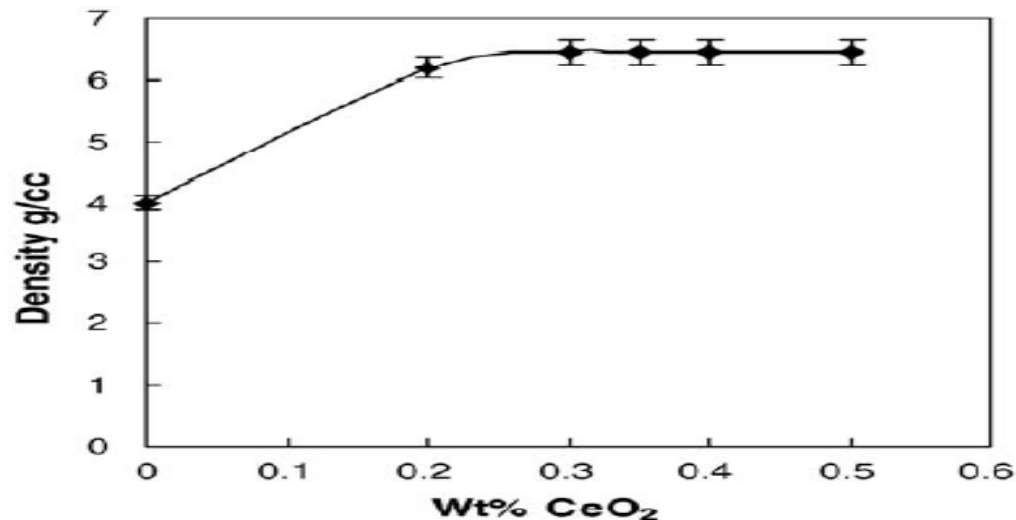


Fig. 2.10 The density of BCZN with CeO₂ content vary (Take from Azough et al [35])

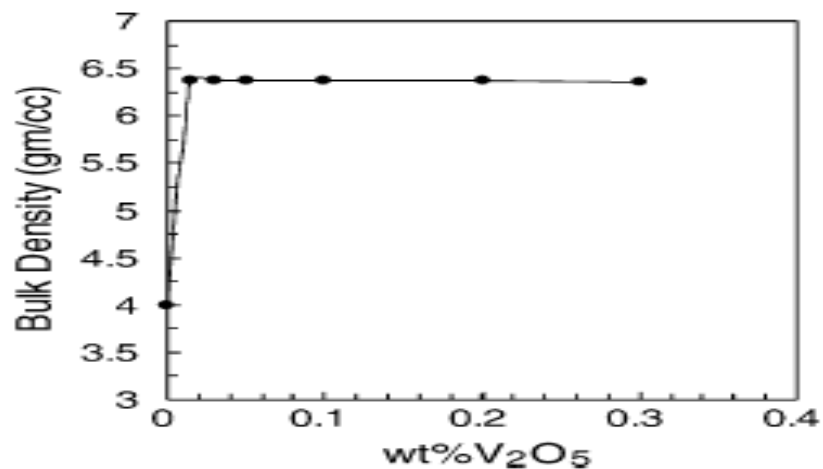


Fig. 2.11 The density of BCZN with V₂O₅ content vary (take from Azough et al [36])

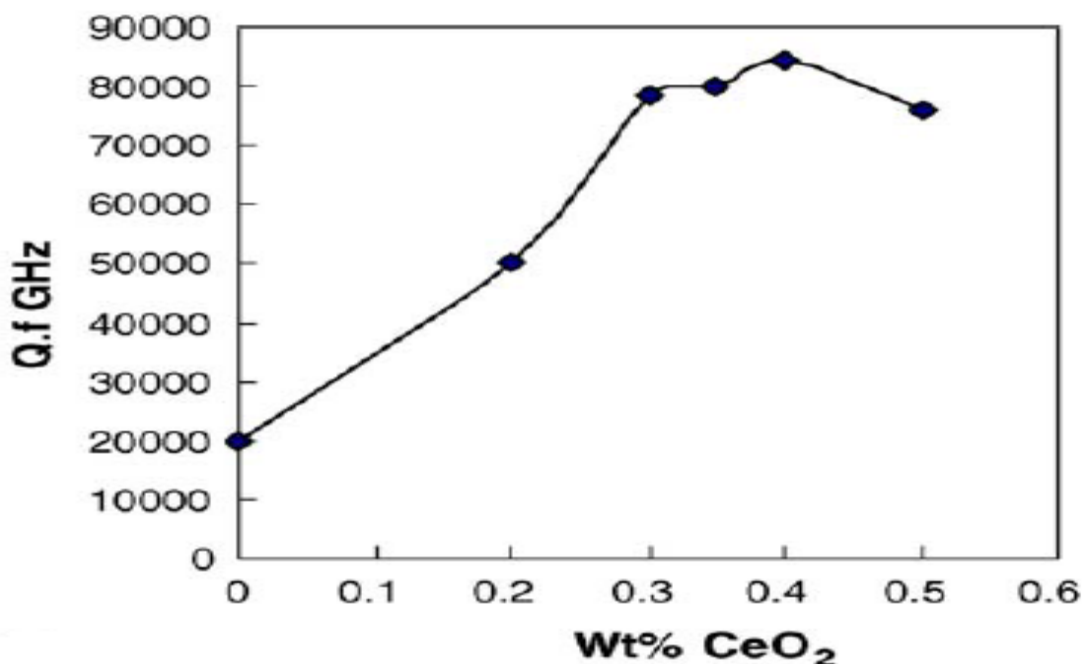


Fig. 2.12 Quality factor vs CeO_2 content in BCZN ceramics (Take from Azough et al [35])

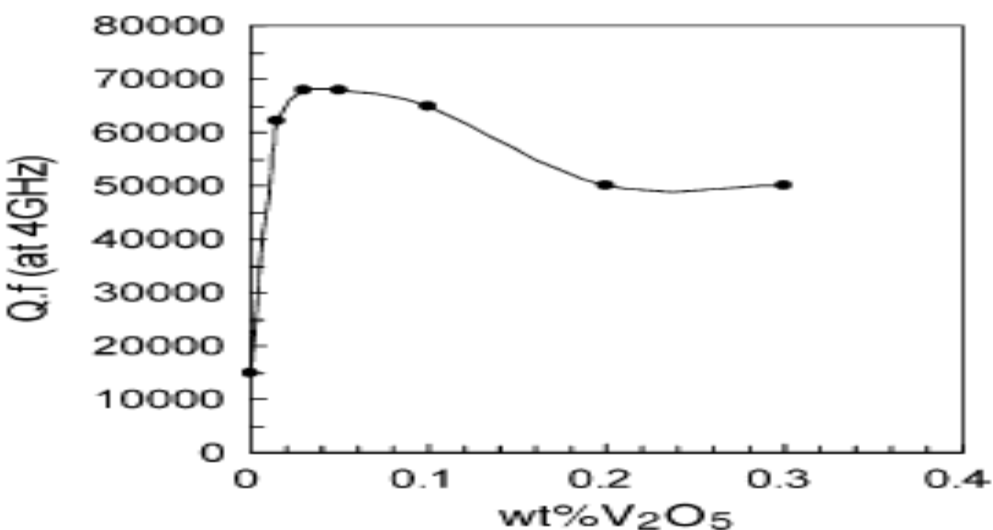


Fig. 2.13 Quality factor vs V_2O_5 content in BCZN ceramics (take from Azough et al [36])

2.7.4 Second phase

With evaporation of elements, there would be second phase growth in the materials.

The second phase plays an important role in dielectric properties. Freer et al [6] indicated there are three phases are present in BZN ceramics after sintering at 1550°C. Except for the main phase, two second phases emerge on the surface phase. They are $\text{Ba}_8\text{ZnNb}_6\text{O}_{24}$ (Zn-deficient phase) which has excellent dielectric properties of quality

factor ($Q \times f_0 > 56,000$) and a positive temperature coefficient of resonant frequency (+35 ppm/ $^{\circ}\text{C}$) and $\text{Ba}_5\text{Nb}_4\text{O}_{15}$ (Zn-free) which has good dielectric properties of $Q \times f_0 = 52,000$ and +70 ppm/ $^{\circ}\text{C}$. As the dielectric properties tend to decrease when those two phases are removed, they appear to give advantages to dielectric properties. However, second phase might appear when the composition change [38], Hughes et al [38] examined surface phase changes in the BZN-BGT system. The result showed that the second phase would grow with the increase amount of BGT content, for example the thickness of the second phase with 20% BGT doping is two times that in pure BZN ceramics.

CHAPTER III

EXPERIMENT PROCESSING AND ANALYSIS

METHODS

3.1 Preparation of materials

Table 3-1 shows the background information on the samples used in this project. All the samples are based on $\text{Ba}(\text{Co}_{0.7}\text{Zn}_{0.3})_{1/3}\text{Nb}_{2/3}\text{O}_3$. They were prepared by the company Powerwave in the form discs. Specimens can be divided in term of sinter schedule from 4h, 12h, 16h and 24h, diameter 17mm to 35.6mm, as well as different heights which are 4.82mm, 10.9mm and 14mm. The basic dielectric properties were in the following ranges: quality factor from 12119 GHz to 99976 GHz, Tcf from -2.71 ppm / °C to +6.15 ppm / °C. All the specimens exhibited >95% theoretical density around 6.2 gm/cc.

Table 3.1 Specimen in this project

| | Sinter time | Q value | f ₀ (MHz) | Q _{xf} (Ghz) | Tcf | OD (mm) | Ht (mm) | Area | Density |
|-----|-------------|---------|----------------------|-----------------------|-------|---------|---------|------|---------|
| s1 | 1450/4h | 45150 | 2214.3 | 99976 | 3.48 | 35.4 | 4.82 | 9.84 | 6.10 |
| s2 | 1450/4h | 13600 | 1689.2 | 22973 | 5.34 | 35.6 | 10.9 | 9.95 | 6.24 |
| s3 | 1450/4h | 7700 | 1573.9 | 12119 | 6.15 | 35.5 | 14 | 9.90 | 6.28 |
| s4 | 1450/12h | 9830 | 1578.5 | 15517 | 5.95 | 35.5 | 14.1 | 9.90 | 6.23 |
| s5 | 1450/16h | 41500 | 1580.42 | 65587 | 5.09 | 35.5 | 14.1 | 9.90 | 6.23 |
| s6 | 1450/16h | 25800 | 3156.23 | 81431 | 3.44 | 17 | | | 6.278 |
| s7 | 1450/16h | 23730 | 3200.03 | 75937 | -2.71 | 17 | | | 6.285 |
| s8 | 1450/24h | 51000 | 1581.4 | 80651 | 5.02 | 35.6 | 14 | 9.95 | 6.24 |
| s9 | 1450/4h | 48650 | 1596.3 | 77660 | -1.33 | 35.5 | 13.9 | 9.90 | 6.34 |
| s10 | 1450/24h | 43000 | 1601.86 | 68880 | -1.43 | 35.5 | 14 | 9.90 | 6.29 |

In the study, sample preparation can be divided into three parts by analysis method: (1) for X-Ray diffraction, (2) optic microscopy, (3) scanning electron microscopy. In the beginning of sample preparation, all the samples were cut in half, then cutting 5mm from each half sample. One of them is for X-ray diffraction and the other for

microscopy. Otherwise, preparation processes include cold mount, grinding, polishing and colloidal silica polishing.

A. For X-Ray diffraction:

In this part, specimens only need to grind with Sic 1200 paper after cutting, to make sure the specimens are flat.

B. For optical microscopy:

After the initial cutting, take one slice and cut in half, then using cold mount one half. The processing of cold mount is: put specimens in bottom of oval container with mixed epoxy. Specimen will form as a disc after 24hour, and it need to grind with Sic 60 paper in mount surface and with Sic 1200 paper in materials surface to make sure both two surface are flat. Polishing is following after grinding, the material surface need to polish with $1\mu\text{m}$ diamond disc about 15 minutes to reduce the scratch. Finally, the specimen need to do colloidal silica polishing around 15minutes, after this process, the phases and grain boundary can be seen under optic microscopy.

C. For scanning electron microscopy using:

All the steps are similar as specimen preparation for optic microscopy using, except carbon coated. Before sample analysis in the scanning electron microscopy, sample must be coated with platinum in surface in order to increase the conductivity. This step can avoid unclear image due to remove residual charge in surface.

3.2 Specimen analysis technique

3.2.1 XRD

This study used X-Ray diffraction analysis to understand the phases present and crystal structures present in the specimen. The fundamental principle of X-Ray diffraction is based on Bragg's law. In this project, there was two X-Ray diffraction machine be used to surface phase and ordering degree analysis, each was X'pert MPD diffractometer (Fig. 3-1) and Philips X'pert-1 (Fig. 3-2). The operation conditions are shown as table 3.1 and 3.2. . The main different between those two machine is the wavelength of incident beam, according to Bagg's law ($\lambda = 2ds\sin\theta$), due to the d-space are the same, so the

angle of scanning range need to be modified. Finally, XRD results were compare with ICDD-PDF (International Centre for Diffraction Data-Powder Diffraction File) to understand crystal structure and phase present in the specimen. Otherwise, in order to obtain the ordering degree, there are three areas (shown as Fig. 3-3) to be selected in the middle of the sample. The selected areas will do the XRD under the specific angle around 15° to 35° when X-ray source is $\text{CuK}\alpha(\lambda= 1.788965\text{\AA})$ or 20° to 41° when it is $\text{CuK}\alpha(\lambda= 1.5406 \text{\AA})$.



Fig. 3-1 X'pert MPD diffractometer



Fig. 3-2 Philips X'pert-1

Table 3.2 Operation condition in X'pert MPD diffractormeter

| | |
|---------------------|---|
| X-ray source | CoK α ($\lambda = 1.788965\text{\AA}$) |
| Monochromator | Graphite |
| Operation voltage | 50kV |
| Operation current | 30mA |
| Scanning speed | 0.05/sec |
| Time per step | 10 sec/step |
| Range of 2 θ | 15–35 |

Table 3.3 Operation conditions in Philips X'pert-1.

| | |
|---------------------|---|
| X-ray source | CuK α ($\lambda = 1.5406\text{\AA}$) |
| Monochromator | Graphite |
| Operation voltage | 50kV |
| Operation current | 40mA |
| Scanning speed | 0.05/sec |
| Time per step | 10 sec/step |
| Range of 2 θ | 20–41 |

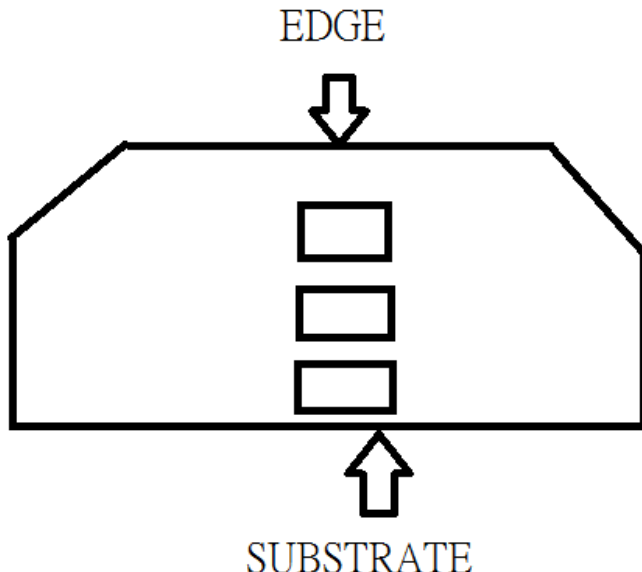


Fig. 3-3 Selected areas for XRD.

3.2.2 Optical Microscopy

The function of optic microscope is similar as scanning electron microscope, but its magnification is lower than SEM. Due to this, SEM would be used as the main analytical tool, optic microscopy as a tool for verification to make sure the date is match to SEM.

In this study, Olympus BH2-OMA (Fig. 3-4) was be used in this project and the magnification range from 5X to 100X. The picture took around 9 main areas shown as Fig 3-5. In addition, there are three additional areas around the edge surface in order to verify the date with SEM.



Fig. 3-4 Olympus BH2-OMA

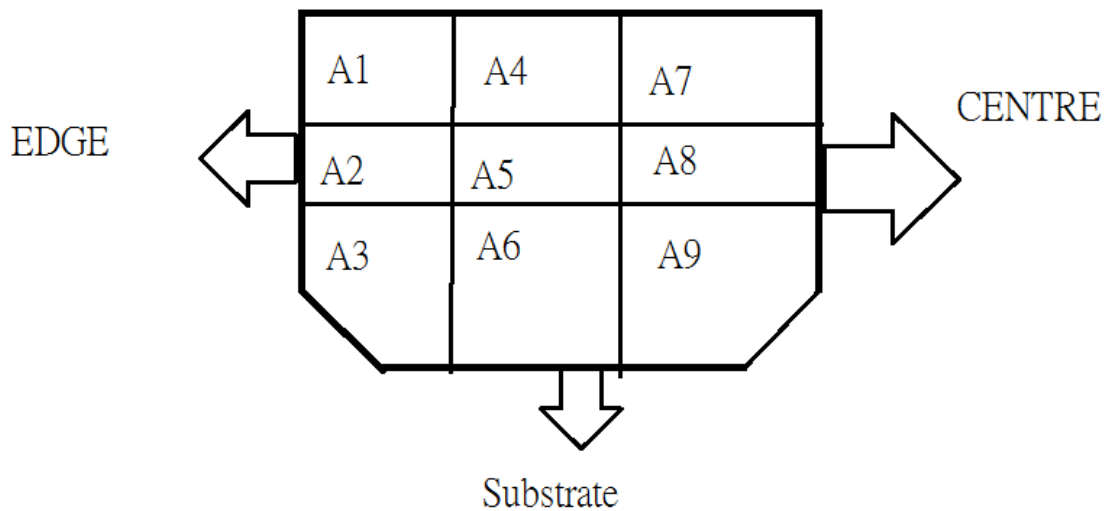


Fig. 3.5 Selected areas for optical microscopy

3.2.3 Scanning Electron Microscopy (SEM)

Scanning Electron microscopy can be used to observed the microstructure, due to it can clearly and easily observe the complete microstructure of the sample. Scanning Electron Microscope (SEM) is using the incident electron reflection on the objects to

understand the surface microstructure; it can do high-rate analog amplification, such as an enlarged optical microscope, let the specimen easy to observe. In this project, FESEM Philips XL30 (Fig. 3-6) was used and the operation conditions are shown in table 3.4. images were collected from the edge to middle in the edge surface,as well as the matrix.



Fig. 3-6 FESEM Philips XL30

Table 3.4 SEM operation conditions

| | |
|-------------------|--|
| Working distance | 10.0 |
| Detector mode | Back scatter electron & Secondary electron |
| Spot size | 3.0 |
| Operation voltage | 8kV to 20kV |
| Magnification | 100X to 1600X |

CHAPTER IV

RESULT AND DISCUSSION

In this project, $\text{Ba}_3\text{Co}_{0.7}\text{Zn}_{0.3}\text{Nb}_2\text{O}_9$ (BCZN) series dielectric ceramics are main materials to be studied. In order to clearly understand factors that influence the dielectric properties, as well as to observe the change in the dielectric properties when processing conditions are varied; therefore the result will be divided into five parts with different conditions namely they are the sintering time, thickness, volume and composition, and will be discussed respectively. All the sections contain phase analysis, crystal structure, microstructure, as well as the relationship between ordering degree and microwave dielectric properties.

4.1 The effect of thickness on the BCZN ceramics

In this group, all samples have the same sintering schedule with the sintering time at for 4 hours, but with different thicknesses. Qxf values were 99976 GHz, 22973 GHz and 12119 GHz, and belong to S1, S2 and S3, respectively. Fig. 4-1 illustrates the trend of Qxf value with respect to thickness. Qxf value changes dramatically between S1 and S2 with about 4.5 times gap, in which the thickness goes down from 10.9mm to 4.82mm.

4.1.1 Phase analysis

Fig. 4-2 shows the result of X-ray diffraction pattern of BCZN series dielectric ceramics with various thicknesses in the surface phase. There are three phases in this material, including BCZN, $\text{Ba}_8(\text{Co},\text{Zn})_1\text{Nb}_6\text{O}_{24}$ and $\text{Ba}_5\text{Nb}_4\text{O}_{15}$ phases. The 1:2 ordering reflection peak appear around $2\theta=17.6^\circ$, but it was not clear on the XRD pattern. However, the main peaks are present in angle with thickness changed, in which the main peaks of S1 and S2 appear in $2\theta=30.9^\circ$ and $2\theta=38.1^\circ$ belong to BCZN phase, and S3 appear in $2\theta=43.7^\circ$ belong to $\text{Ba}_8(\text{Co},\text{Zn})_1\text{Nb}_6\text{O}_{24}$ phase. Otherwise, the grains present both hexagonal structure which has 1:2 ordering degree in B-site and cubic structure which

can be seen as a disorder structure [35]. The relationship between relative intensity of $\text{Ba}_8(\text{Co},\text{Zn})_1\text{Nb}_6\text{O}_{24}$ phase and thickness can be found in Fig. 4.2, relative intensity of $\text{Ba}_8(\text{Co},\text{Zn})_1\text{Nb}_6\text{O}_{24}$ phases tend to increase when thickness goes up. When compare to quality factor, the results clearly shown Qxf value might be decreased with relative intensity of $\text{Ba}_8(\text{Co},\text{Zn})_1\text{Nb}_6\text{O}_{24}$ phase increase. Therefore, Qxf value can be improved with the sample thickness reduced, due to enough thermal processing might remove $\text{Ba}_8(\text{Co},\text{Zn})_1\text{Nb}_6\text{O}_{24}$ phase. In addition, $\text{Ba}_5\text{Nb}_4\text{O}_{15}$ phase tends to disappear gradually with thickness lessen, but there is no evident show the $\text{Ba}_5\text{Nb}_4\text{O}_{15}$ phase has negative effect to Qxf due to it do not have dramatically change $\text{Ba}_8(\text{Co},\text{Zn})_1\text{Nb}_6\text{O}_{24}$ phase in this group.

4.1.2 Microstructure analysis

Fig. 4-3 demonstrated SEM micrograph of the edge surface of BCZN series ceramic which sintering at 1450°C for 4 hours with varied thickness; the graph agreed the X-ray diffraction results. Except the main phase present in the matrix, there are two secondary phases emerge at the sample surface, in which Zn evaporation might result in generation of secondary phase. Freer et al [6] indicate the second phases should be Zn-deficient, $\text{Ba}_8(\text{Co},\text{Zn})_1\text{Nb}_6\text{O}_{24}$, and Zn-free phase, $\text{Ba}_5\text{Nb}_4\text{O}_{15}$. Otherwise, the graph also shows that most grains are show hexagonal in morphology in the matrix, and present as needle-shaped on the surface. At the same time, the densities of secondary phases tend to decline with the reduction in thickness of the sample and the length of needle phase has similar length about 60 to 70 μm . Fig. 4-4 to Fig. 4-6 show optic microscopy image of the internal materials, and all images took in the centre area form substrate to edge. Fig. 4.7 summarized the grain size of each sample, in which the grain size are about 30.5 μm when the thickness of sample from 4.82mm to 10.9mm, and decreased to 28.5 μm when the thickness increased to 14.1mm. Basically, grain size in this group is not significantly different, and it is possible the disparity of grain size between each sample might result from grain shape. In Yoon et al [39] studied, they pointed out ordering degree in B-site might be a crucial factor impact to Qxf value in complex perovskite A ($\text{B}'_{1/3}\text{B}''_{2/3}$) O_3 ceramics, in which Qxf value could be improved with the ordering degree rise. The picture roughly shows there are more and more

cubic structure emerge when the thickness reduce. However, in order to accurately understand the change of ordering degree, it will further discuss with XRD results in next section. In addition, due to all the samples achieve over 95% theoretical density, the density between 6.10 to 6.28, porosity did not have significant change in each sample.

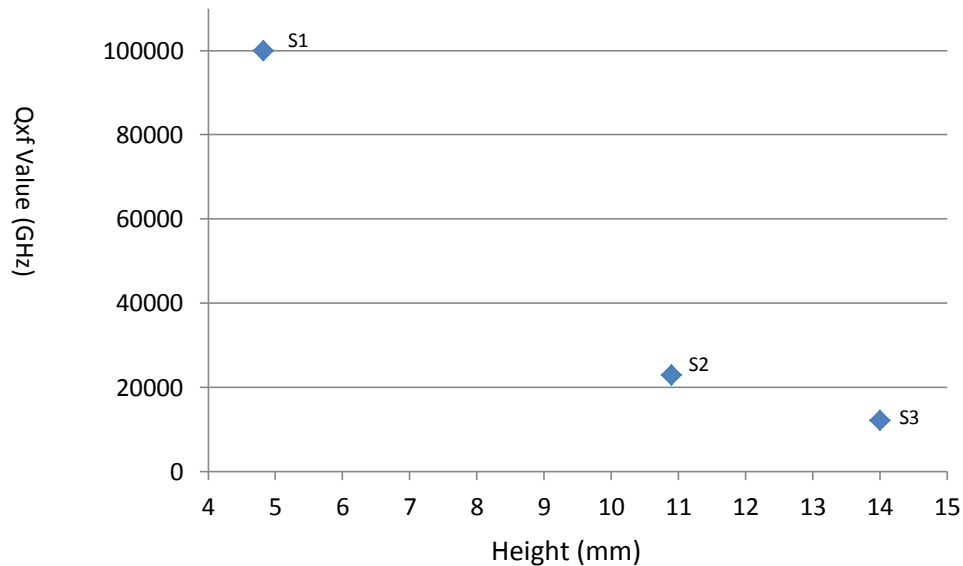


Fig. 4-1 Qxf value as a function of thickness.

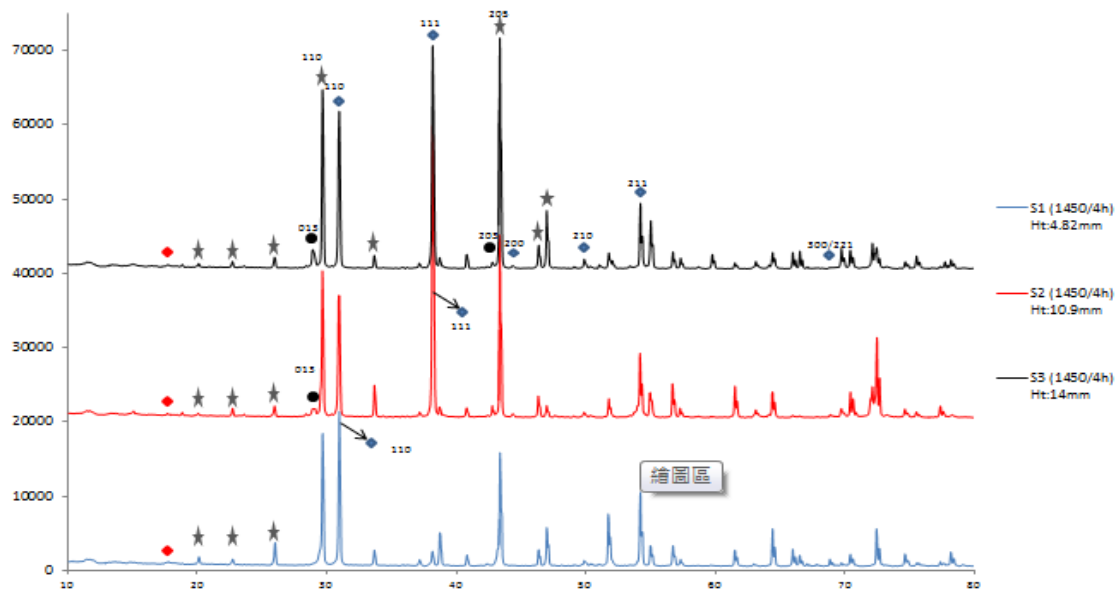


Fig. 4-2 XRD pattern of $\text{Ba}_3\text{Co}_{0.7}\text{Zn}_{0.3}\text{Nb}_2\text{O}_9$ series at various thicknesses. The samples were sintering at 1450°C for 4 hours. (◆: superlattice, ◆: $\text{Ba}_3\text{Co}_{0.7}\text{Zn}_{0.3}\text{Nb}_2\text{O}_9$ (BCZN) phase, ★: $\text{Ba}_8(\text{Co},\text{Zn})_1\text{Nb}_6\text{O}_{24}$ phase, ●: $\text{Ba}_5\text{Nb}_4\text{O}_{15}$ phase).

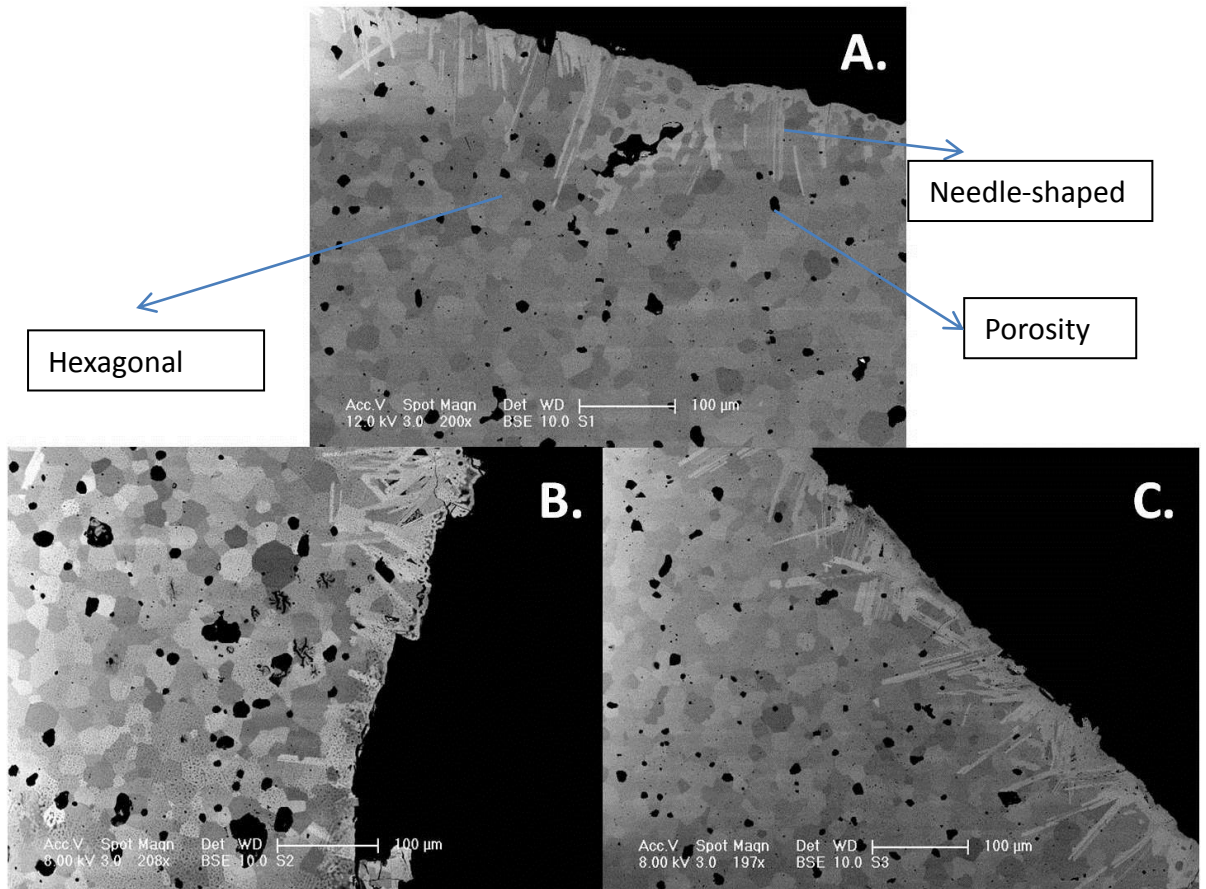


Fig. 4-3: SEM photographs of specimens with different thicknesses sintered at 1450 °C/4 h.

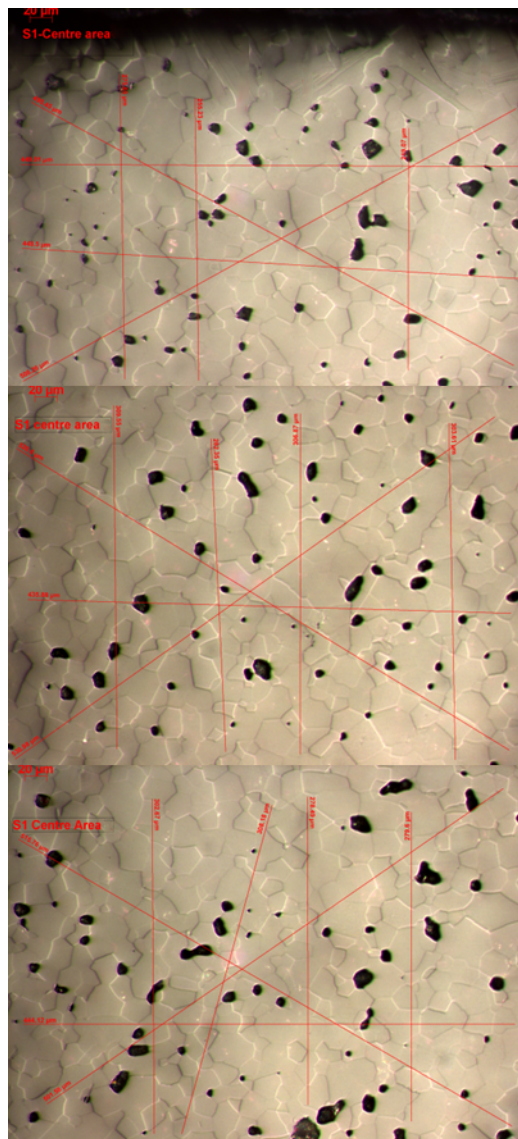


Fig. 4-4 Optical microscopy photographs of S1.

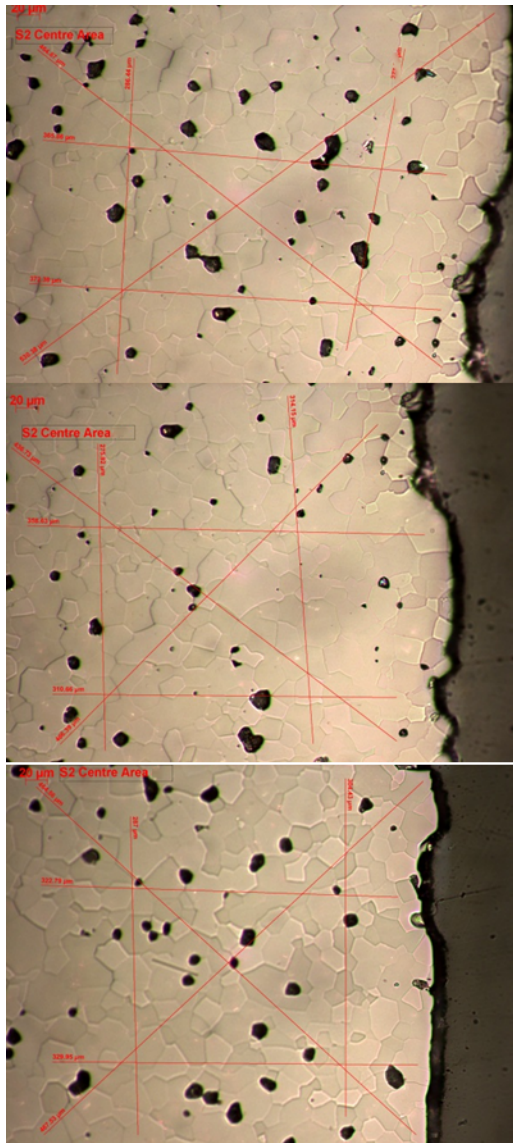
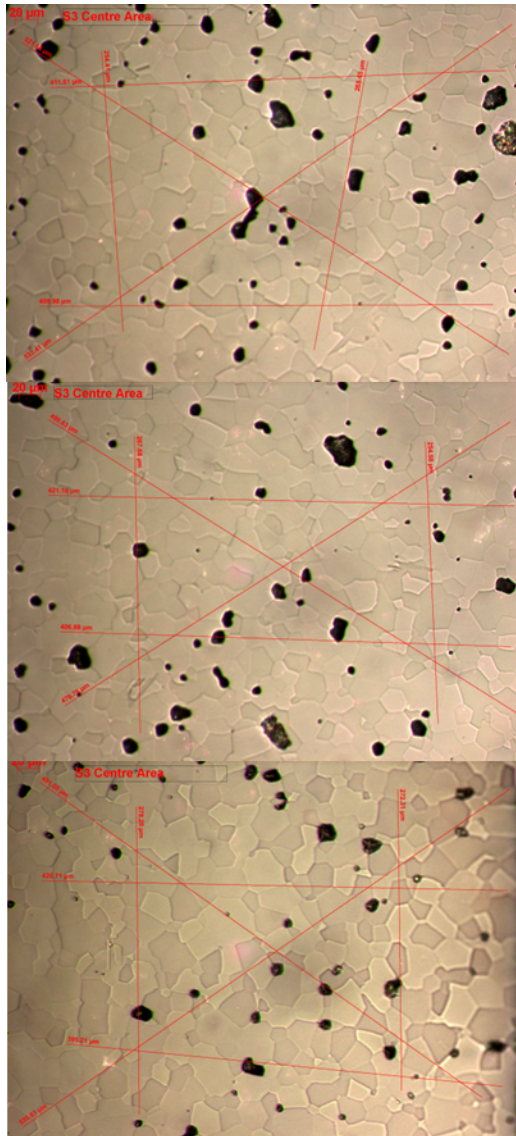


Fig. 4.5 Optical microscopy photographs of S2.



EDGE 28.11 μ m

Middle 27.92 μ m

Substrate 28.07 μ m

Fig. 4.6 Optical microscopy photographs of S3.

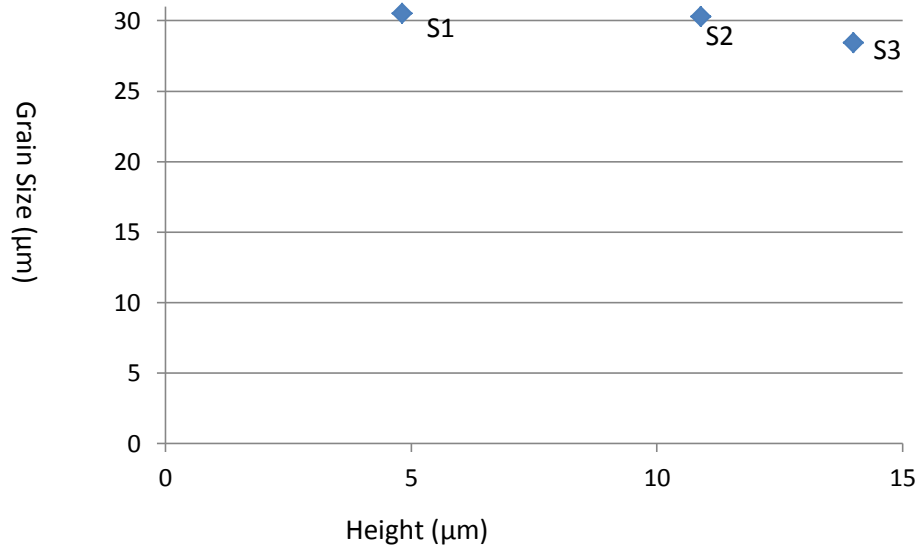


Fig. 4.7 Grain size as a function of thickness.

4-2 The effect of sintering time on the BCZN ceramics

Sintering time is variable in this group. Fig. 4-8 show the trend of Qxf value varied from 12119 GHz, 15517 GHz, 65587 GHz and 80651 GHz due to sintering time increased. The result shows Qxf value has a greater gap between S4 and S5, Qxf value in S5 which sintering at 1450°C for 16 hours is 4 times bigger than it in S4 which sintering at 1450°C for 12 hours.

4.2.1 Phase analysis

In this group, except S3, all the XRD patterns have similar structure, and the main peaks appear in $2\theta=38.1^\circ$ belong to BCZN phase when sintering time more than twelve hours (Fig 4-9). The figure clearly show the trend between BCZN and $\text{Ba}_8(\text{Co},\text{Zn})_1\text{Nb}_6\text{O}_{24}$ phases, in which the relative intensity of BCZN incline to go up with sintering time increase, in other words , the relative intensity of $\text{Ba}_8(\text{Co},\text{Zn})_1\text{Nb}_6\text{O}_{24}$ phase are go down. However, the relative intensity of (110) between BCZN $\text{Ba}_8(\text{Co},\text{Zn})_1\text{Nb}_6\text{O}_{24}$ is worthy to be discussed due to its trend is match to the gradient of Qxf value, in which BCZN phase goes up, Qxf value rise, on the other hand, Qxf value goes down when $\text{Ba}_8(\text{Co},\text{Zn})_1\text{Nb}_6\text{O}_{24}$ phase increase. Moreover, the $\text{Ba}_5\text{Nb}_4\text{O}_{15}$ phase tends to increase with the sintering time rise, and it reaches the maxima when sintering at 1450°C for 16 hours, however, it drop again when the sintering time increase to 24 hours. Otherwise,

regardless of changes in sintering time, there are still three different phases present in the samples.

4.2.2 Microstructure analysis

The variation of secondary phase in the edge of surface phase can be easily observed by SEM image (Fig. 4-10), as well as grain size. There are visible second phase growth at edge of surface, the needle-shaped phase tends to grow deeper with the sintering time reduce from 24 hours to 4 hours, as well as the density of needle-shaped phase increase. The difference of grain size can be clearly indicate in Fig. 4-10A and 4-10D with sintering time change from 4 hours to 24 hours, and the grain size only has a slight change between Fig 4-10B and 4-10C with sintering time increase from 12 hours to 16 hours. With optical microscope images (Fig. 4-6, and Fig 4-11 to Fig 4-13) to further explore the grain size, the results show grain size growth from $28.5\mu\text{m}$ to $50\mu\text{m}$ when sintering time rise from 4 hours to 24hours. In addition, the grain structure tends to harmonization with sintering time go up. In other words, ordering degree might be improved. The trend of grain size change can be summarised as Fig. 4-14, and it might result from the grain growth at liquid state; long sintering time allows for grain growth to occur.

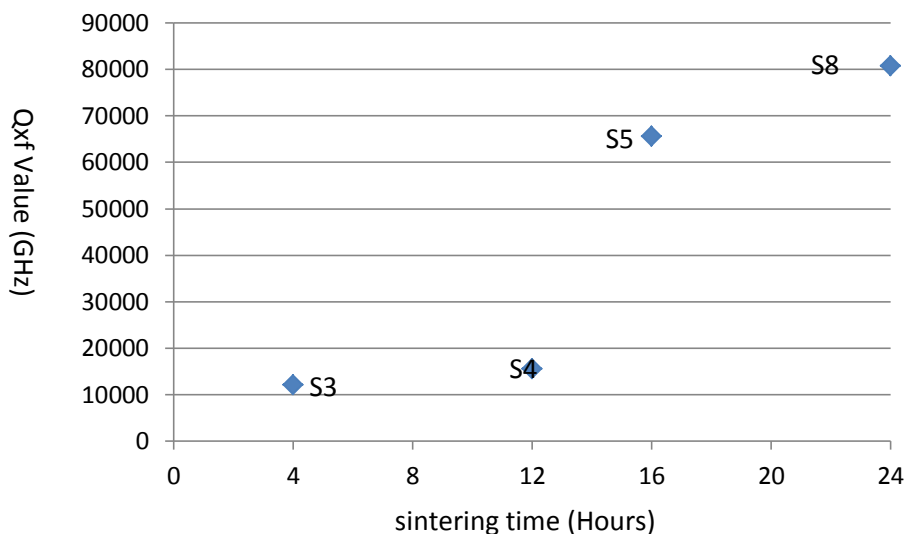


Fig. 4-8: Qxf value as a function of sintering time.

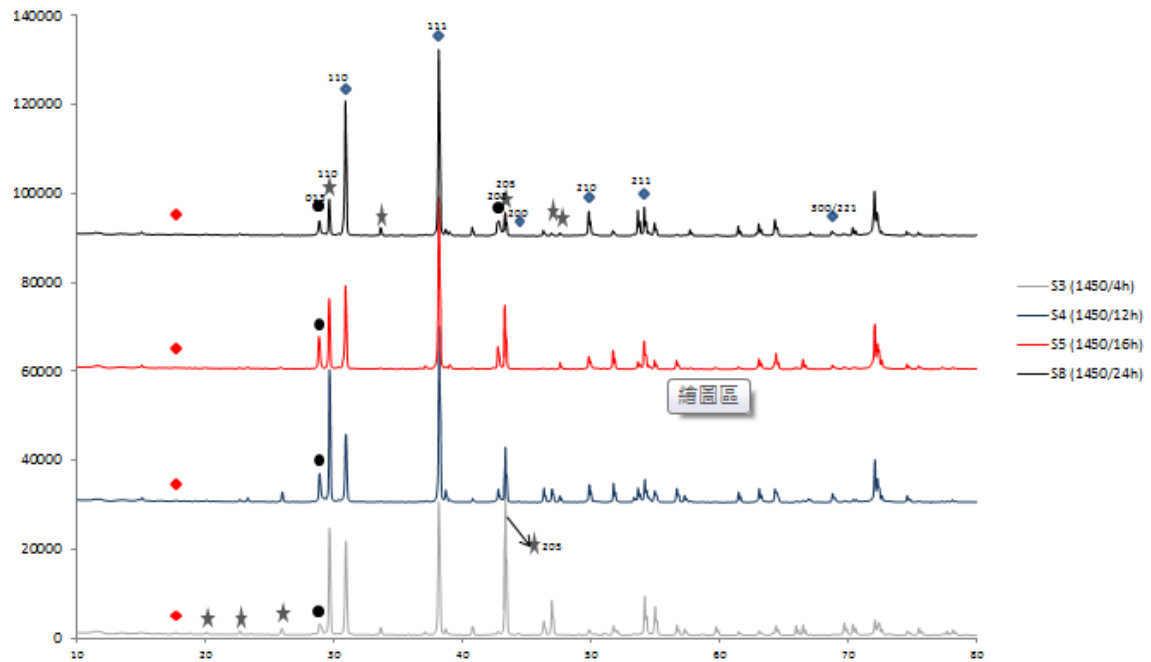


Fig. 4-9: XRD pattern of $\text{Ba}_3\text{Co}_{0.7}\text{Zn}_{0.3}\text{Nb}_2\text{O}_9$ series at various sintering time. The samples were sintering at 1450°C. (◆: superlattice, ◆: $\text{Ba}_3\text{Co}_{0.7}\text{Zn}_{0.3}\text{Nb}_2\text{O}_9$ (BCZN) phase, ★: $\text{Ba}_8(\text{Zn},\text{Co})\text{Nb}_6\text{O}_{24}$ phase, ●: $\text{Ba}_5\text{Nb}_4\text{O}_{15}$ phase.

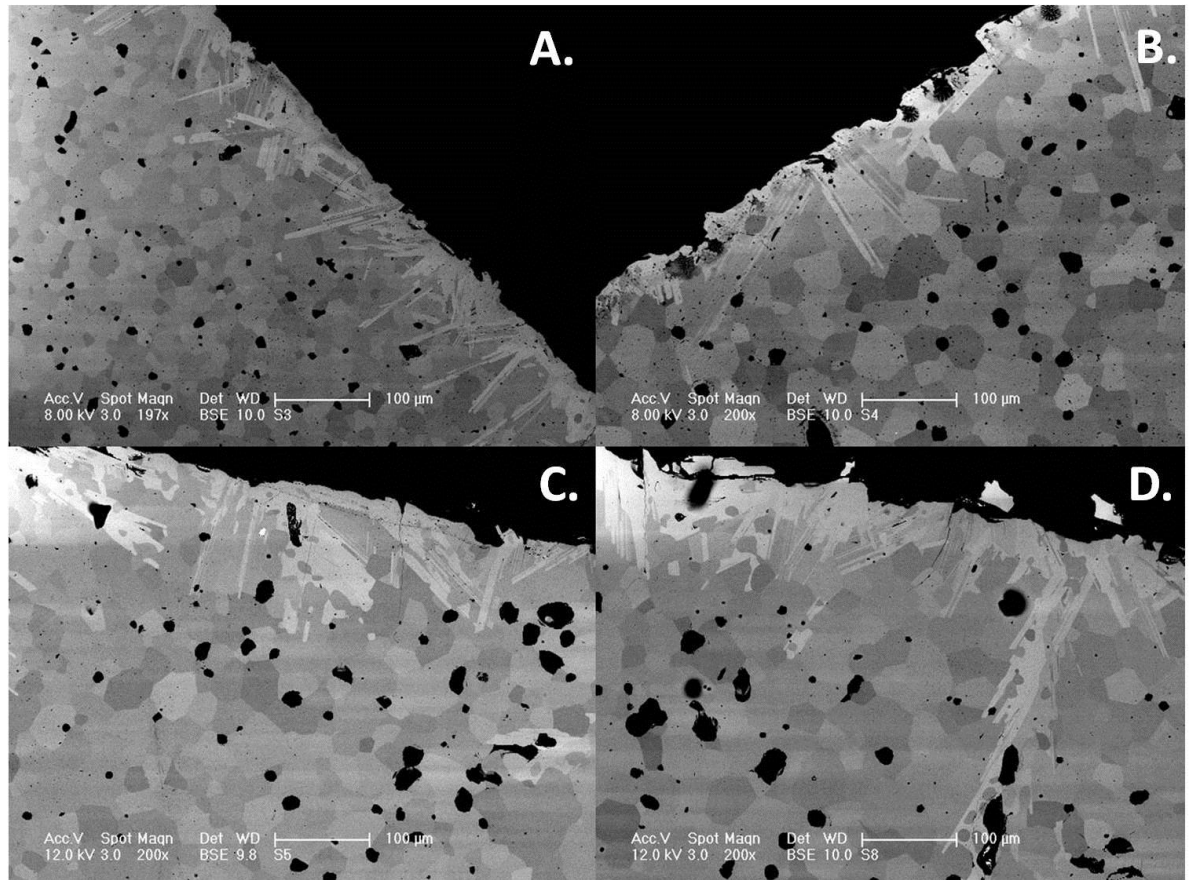
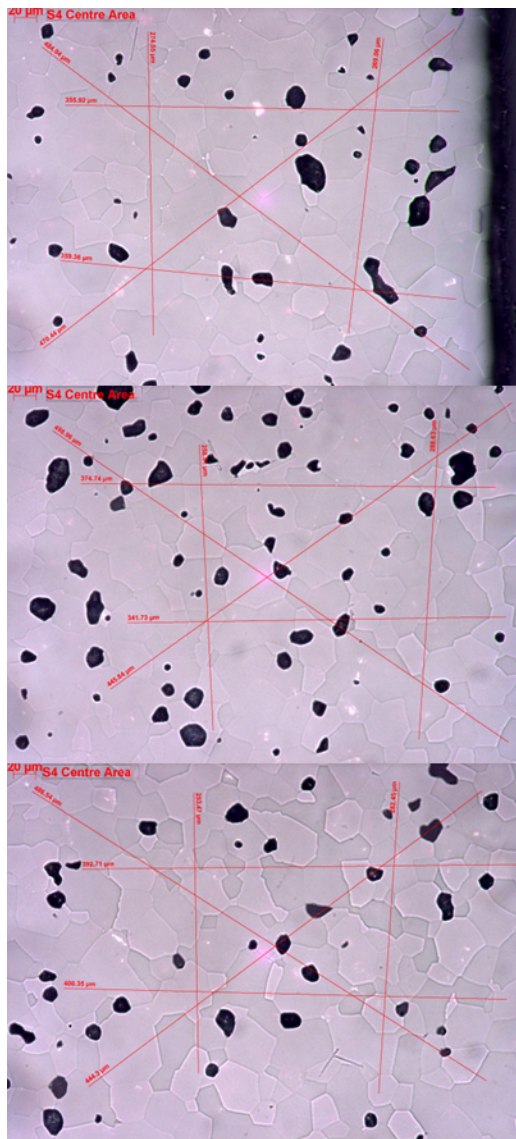


Fig. 4.10 SEM photographs of specimens with different sintering time sintered at 1450 °C.

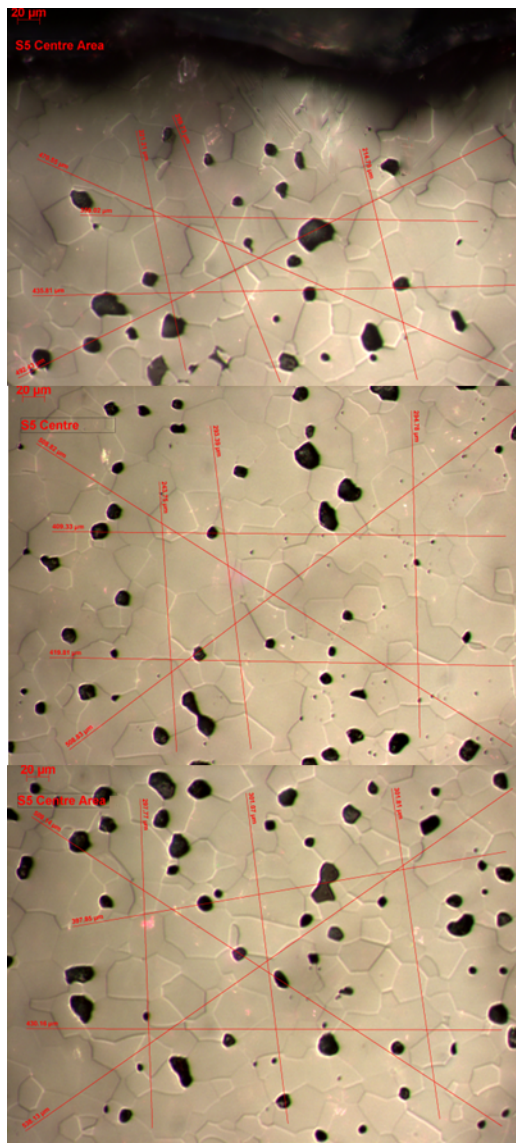


EDGE 46.05 μ m

Middle 39.15 μ m

Substrate 37.50 μ m

Fig. 4-11 Optical microscopy photographs of S4.



EDGE 41.96μm

Middle 41.37μm

Substrate 40.85μm

Fig. 4-12 Optical microscopy photographs of S5.

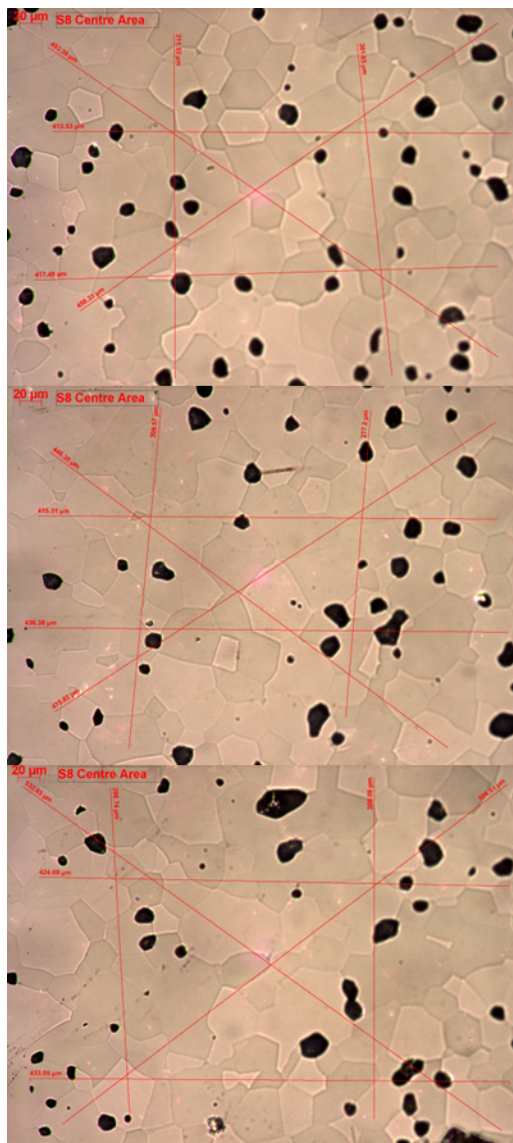


Fig. 4-13 Optical microscopy photographs of S8.

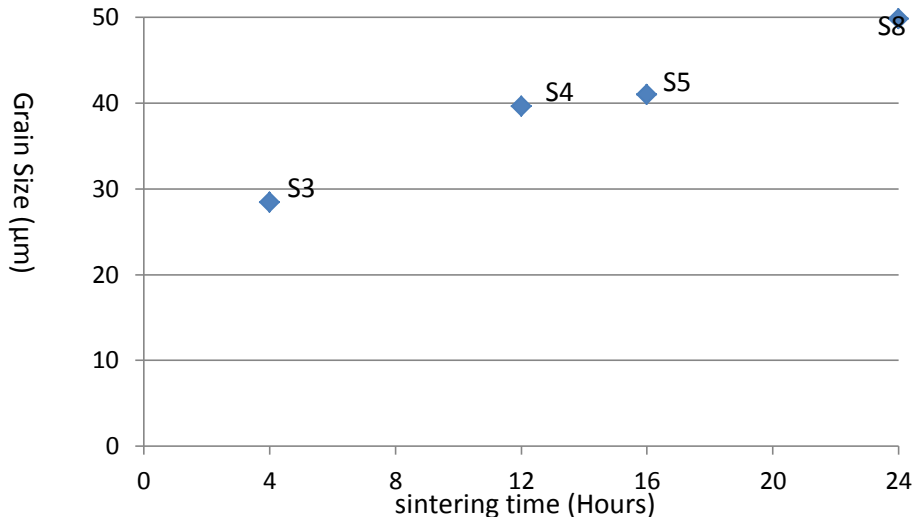


Fig. 4-14: Grain size as a function of sintering time

4.3 The effect of volume on the BCZN ceramics

Fig 4-15 illustrates Qxf value in different volume sintering at 1450°C for 16 hours, the result display the quality factor falls with the area increase, in which Qxf value in S5 is 65587 GHz, and 81431 GHz in S6. Comparing with the diameter and thickness, S5 is twice to S6, in other words, S5 has 8 times volume bigger than S6. Otherwise, the sample discussed in section 4.1 can be seen as volume varied as well. However, the main different should be the area of sample. To compare with S1 and S6, although the sintering time in S6 is bigger than S1, as well as volume smaller in S6, the Qxf value in S1 still greater than S6, it might result from the heating area, as well as the thickness.

4.3.1 Phase analysis

The XRD pattern shows as Fig. 4-16, basically, the XRD pattern structure are similar, except the main phase shift from $2\theta=30.9^\circ$ to $2\theta= 38.1^\circ$ with area varied, both two main peak belong to BCZN phase. Otherwise, the relative intensity of $\text{Ba}_8(\text{Co},\text{Zn})_1\text{Nb}_6\text{O}_{24}$ phases tends to decrease with the area fall, as well as $\text{Ba}_5\text{Nb}_4\text{O}_{15}$ phase.

4.3.2 Microstructure analysis

Fig. 4-15 shows information about grain size agonist to area, the result show area did not have significantly affect to grain size; in which the grain sizes are around $40\mu\text{m}$ in this system. Although there is $2\mu\text{m}$ gap between those two samples, the cause could be traced back to its grain shape and chosen area to calculate. In SEM image (Fig 4-18), there is no significant difference between two samples can be observed, including grain size, porosity and secondary phase, except there are more needle-shaped can be observed in S5 (Fig 4-18 A), the generation of this phenomenon might due to small volume lead sufficient thermal. Fig 4-19 shows optic microscopy image of S6, to compare with Fig 4-12 which is microscopy image of S6, there is no significant different can be observed.

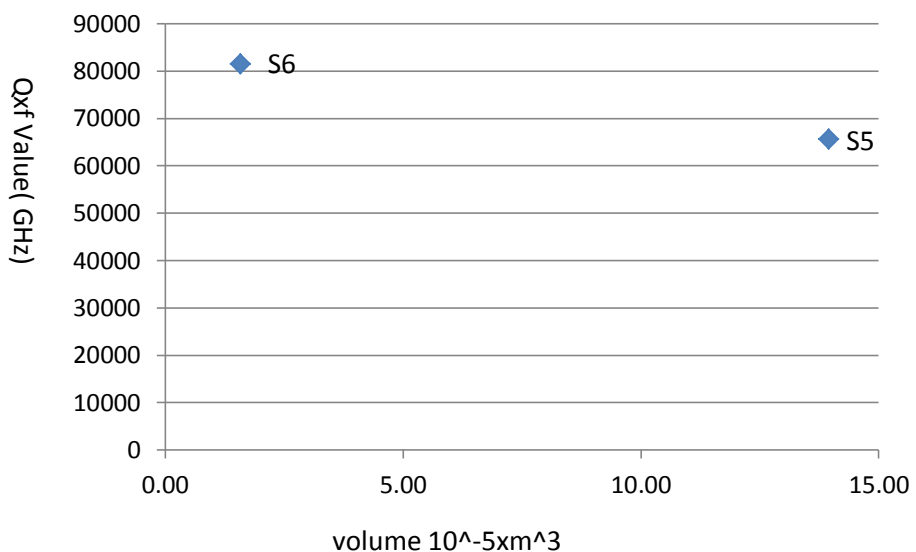


Fig. 4-15: Qxf value as a function of volume

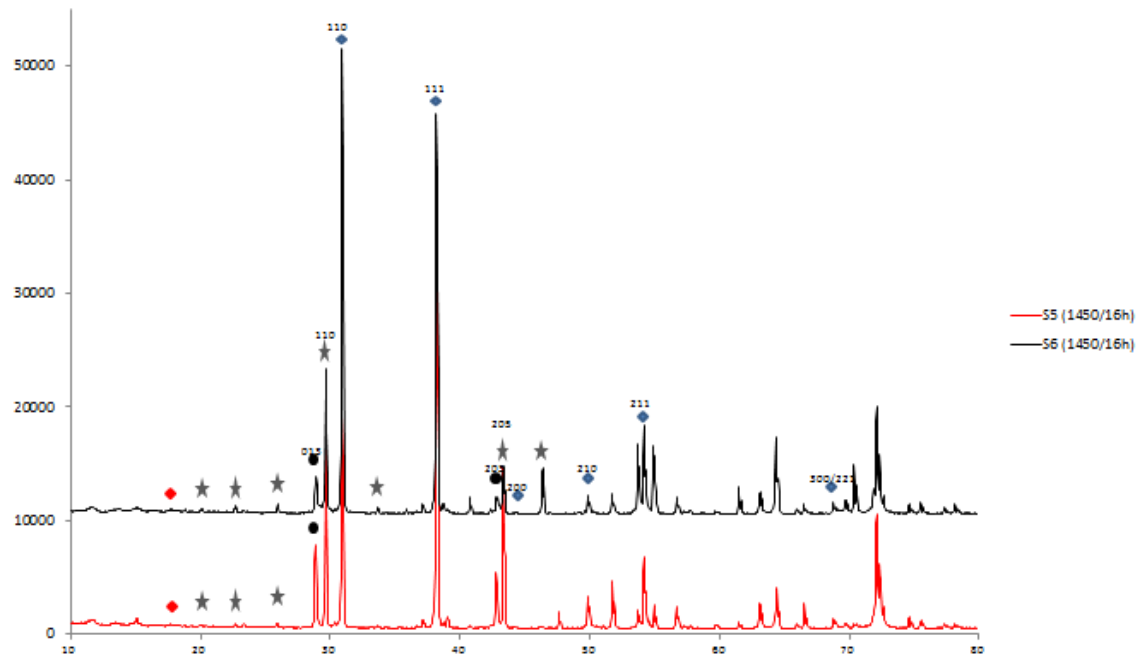


Fig. 4.16: XRD pattern of $\text{Ba}_3\text{Co}_{0.7}\text{Zn}_{0.3}\text{Nb}_2\text{O}_9$ series at various volumes. The samples were sintering at 1450 for 16 hours. (◆: superlattice, ◇: $\text{Ba}_3\text{Co}_{0.7}\text{Zn}_{0.3}\text{Nb}_2\text{O}_9$ (BCZN) phase, ★: $\text{Ba}_8(\text{Co},\text{Zn})_1\text{Nb}_6\text{O}_{24}$ phase, ●: $\text{Ba}_5\text{Nb}_4\text{O}_{15}$ phase.

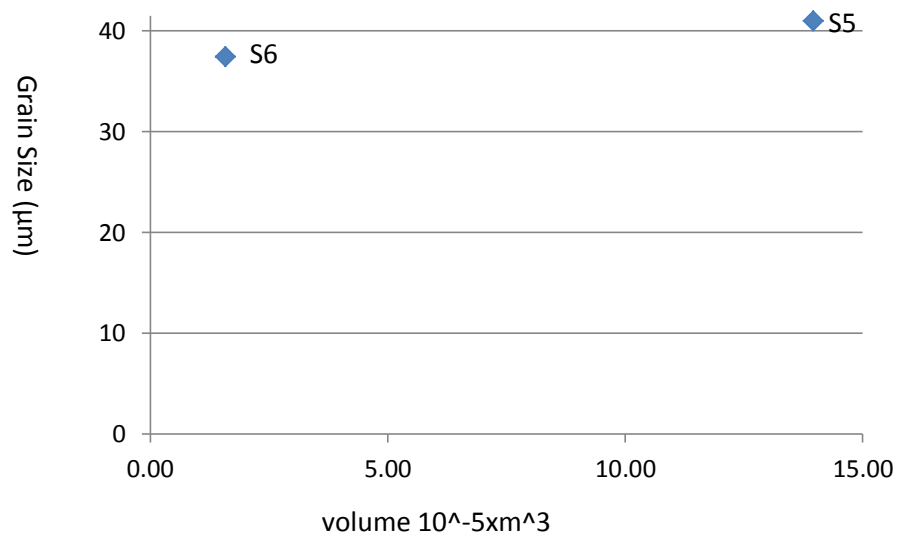


Fig. 4.17: Grain size as a function of volume.

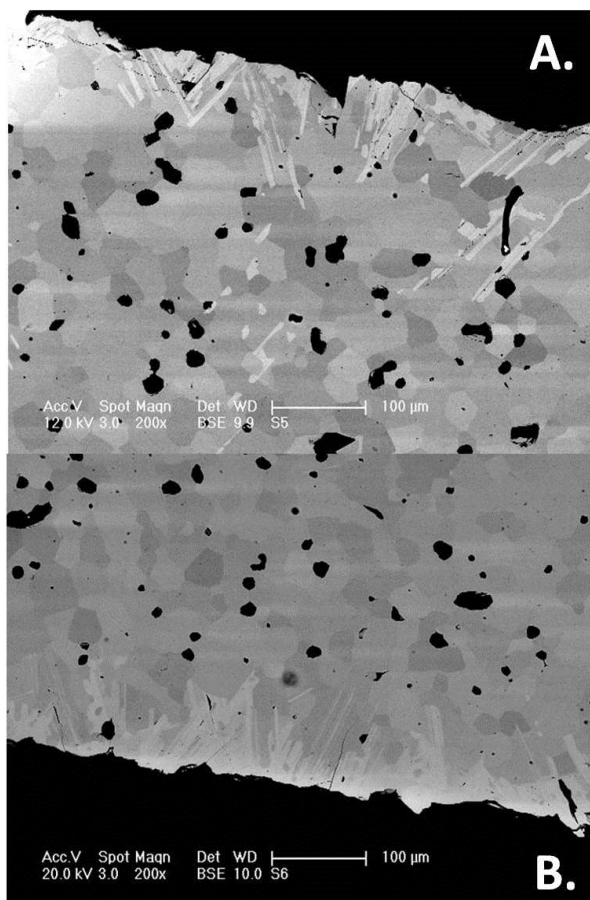


Fig. 4-18 SEM photographs of specimens with different volumes sintered at 1450 °C/16 h.

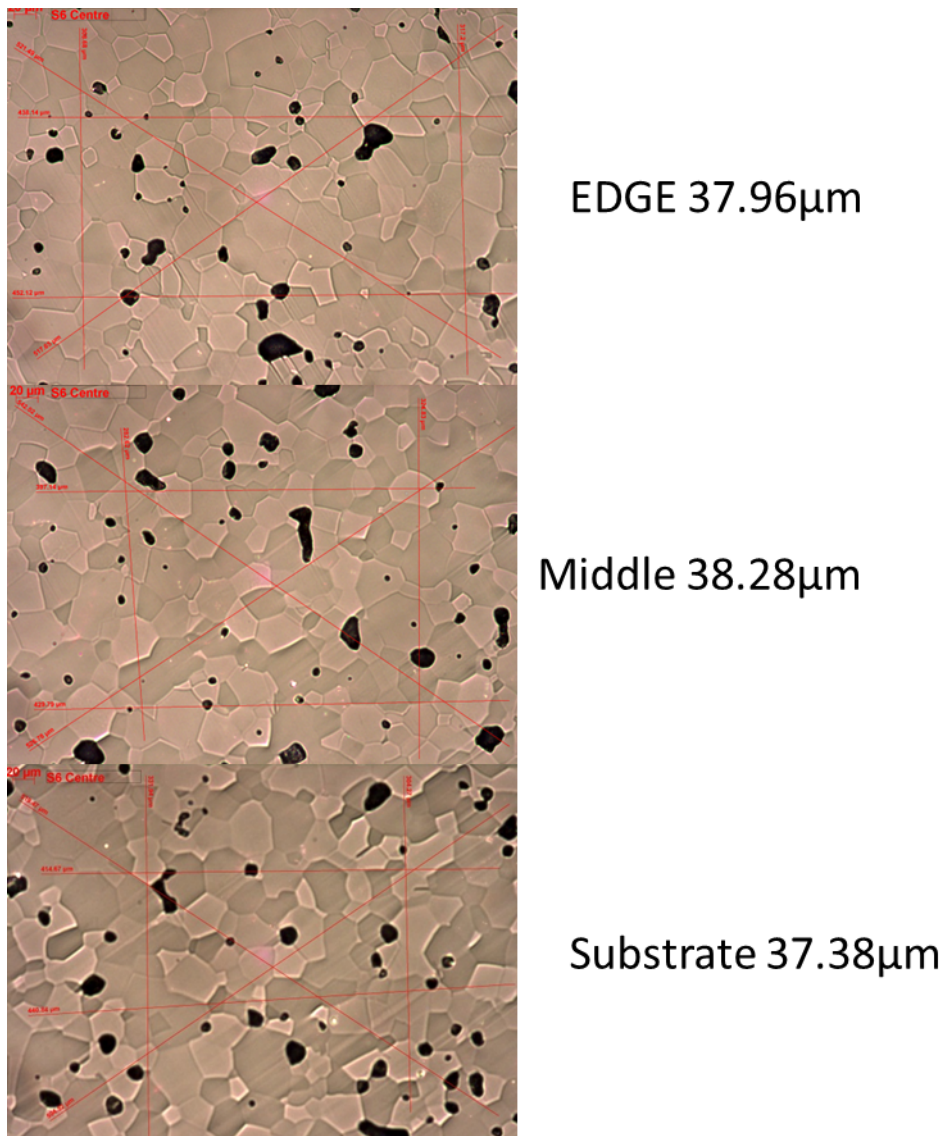


Fig. 4.19 Optical microscopy photographs of S6.

4.4 The effect of processing on the BCZN ceramics

In this section, due to the different processing might cause compositions change slightly, different composition can be seen as a variable; in which S3, S6 and S8 have the same composition, and S7, S9, S10 have similar composition. Therefore, all samples can be divided into three groups by the same sintering schedule; S3 and S9 which sintering at 1450°C for 4 hours, S6 and S7 which sintering at 1450°C for 16 hours, and S8 and S10 which at 1450°C for 24 hours. In addition, S9 and S10 can be seen as an additional group due to them has similar composition but different sintering time. In Fig. 4-20, the data show most samples have a high Q_{xf} value around 70000 GHz or above, except S3.

Otherwise, with the processing changed, the composition has slight different, however, Q_{xf} tend to decrease, except the group S3&S9. Q_{xf} value in S9 is about 6.5 times greater than it in S3. Moreover, in S7, S9 and S10 which have the similar composition, Q_{xf} value seems tend to go up with sintering time reduced.

4.4.1 Phase analysis

Fig. 4-21, 4-22 and 4-23 show the XRD pattern of different group which with the same sintering schedule. According to the figures, it is clearly to show the $\text{Ba}_5\text{Nb}_4\text{O}_{15}$ phase tends to reduce in S7, S9 and S10; in which the peak around $2\theta=28.6^\circ$ and $2\theta=42.7^\circ$ are disappear. In addition, the main peaks appear around $2\theta=30.6^\circ$ belong to BCZN phase in S7 and S9, and it appear around $2\theta=29.6^\circ$ belong $\text{Ba}_8(\text{Co},\text{Zn})_1\text{Nb}_6\text{O}_{24}$ Phase in S10. Otherwise, Fig. 4-24 display the $\text{Ba}_8(\text{Co},\text{Zn})_1\text{Nb}_6\text{O}_{24}$ phase tend to increase with time rise in this composition.

4.4.2 Microstructure analysis

Fig. 25 to Fig. 27 show the SEM micrograph, samples image in the same figure contain the same sintering condition, therefore, it can compare the difference of microstructure with composition change. All the pictures show there are secondary phases present around the edge of surface phase, and the difference of secondary phase between S3 and S9 were clearly shown in Fig 25. The thickness of secondary phase in S9 is about half to S3, otherwise, there are visible secondary phase spread to matrix. The main different of secondary phase between different composition is the structure. In S6, S8 and S9, the secondary phase present as needle-shaped structure, however, it present similar bulk-shaped in S7, S9 and S10. Furthermore, the grain size has dramatically varied with composition change. Fig. 25 shows the BCZN ceramics sintering at 1450°C for 4 hours, however, the grain cannot visible in Fig. 25B, and it can be seen clearly in Fig. 25A with the same magnification. Fig 4-28 and Fig 4-29 show the High-magnification SEM image of S9, the grain sizes are not uniform; in which the biggest grain size around 20μm, and the smallest one might be less than 1μm. Moreover, although Fig. 27 show S8 and S10 which sintering at 1450°C for 24 hours have similar grain size around the edge of surface phase, the grain size varied from

substrate to edge in S10. Fig. 30 illustrates the trend of grain size in S10, in the edge, there are only few small grains emerge, and there are more and more small grains presence in the middle of sample, and almost all grain presence as a small grain in the substrate. However, the microstructure of S6 and S7 did not have momentous variation around the whole sample; it might result from small volume.

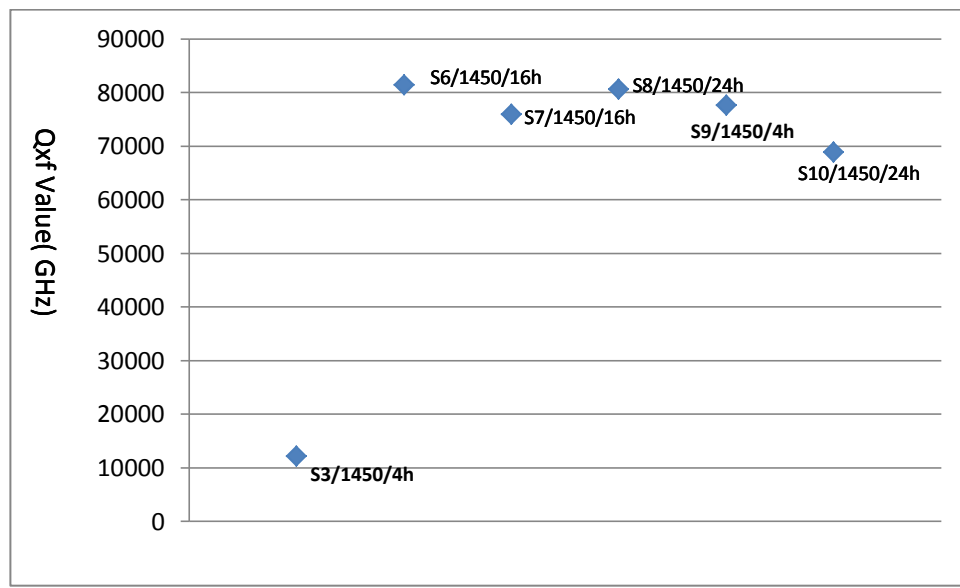


Fig. 4-20: Qxf value.

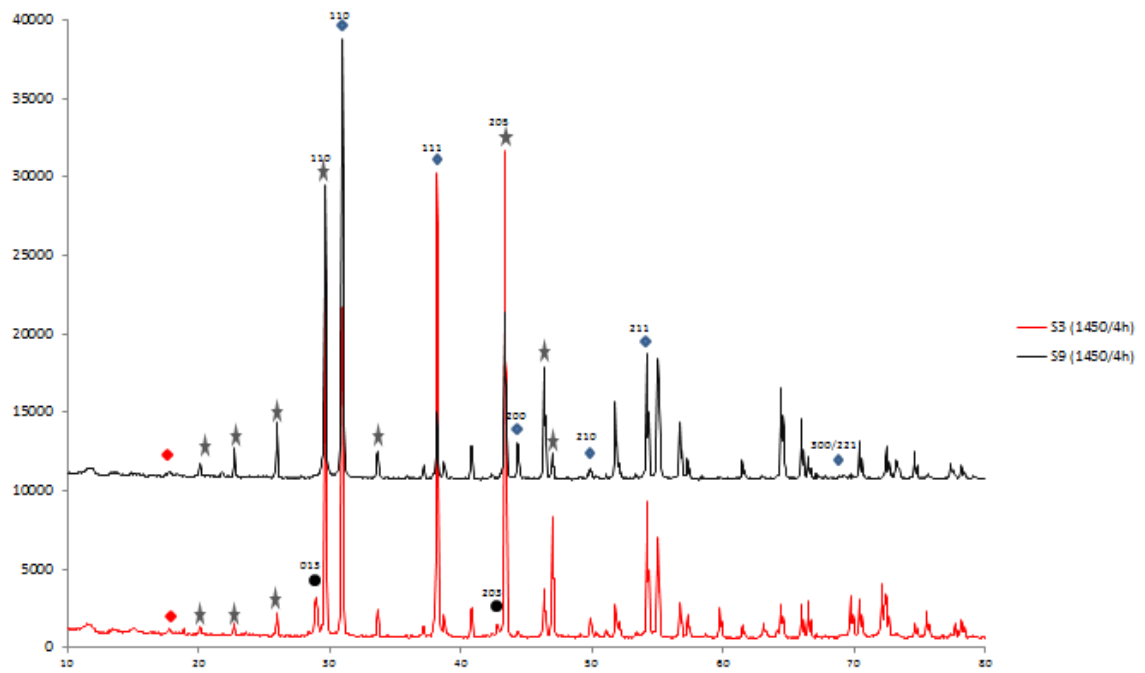


Fig. 4-21: XRD pattern $\text{Ba}_3\text{Co}_{0.7}\text{Zn}_{0.3}\text{Nb}_2\text{O}_9$ series at various compositions. The samples were sintering at 1450°C for 24 hours. (◆: superlattice, ◆: $\text{Ba}_3\text{Co}_{0.7}\text{Zn}_{0.3}\text{Nb}_2\text{O}_9$ (BCZN) phase, ★: $\text{Ba}_8(\text{Co},\text{Zn})_1\text{Nb}_6\text{O}_{24}$ phase, ●: $\text{Ba}_5\text{Nb}_4\text{O}_{15}$ phase).

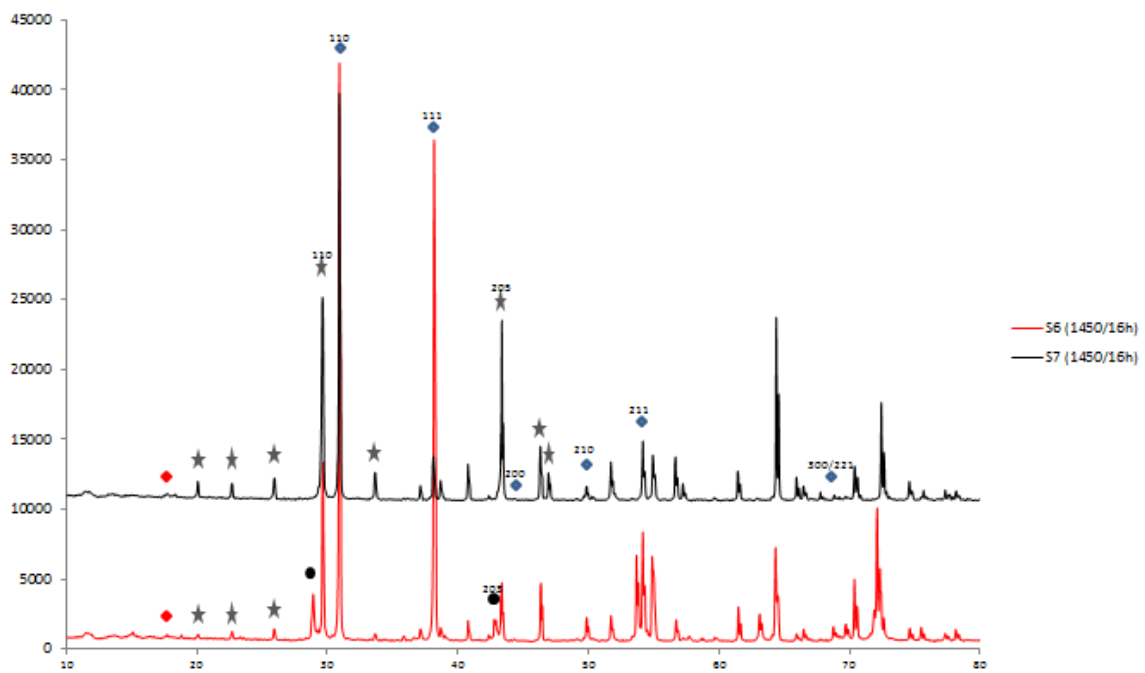


Fig. 4-22: XRD pattern of $\text{Ba}_3\text{Co}_{0.7}\text{Zn}_{0.3}\text{Nb}_2\text{O}_9$ series at various compositions. The samples were sintering at 1450°C for 24 hours (◆: superlattice, ◆: $\text{Ba}_3\text{Co}_{0.7}\text{Zn}_{0.3}\text{Nb}_2\text{O}_9$ (BCZN) phase, ★: $\text{Ba}_8(\text{Co},\text{Zn})_1\text{Nb}_6\text{O}_{24}$ phase, ●: $\text{Ba}_5\text{Nb}_4\text{O}_{15}$ phase).

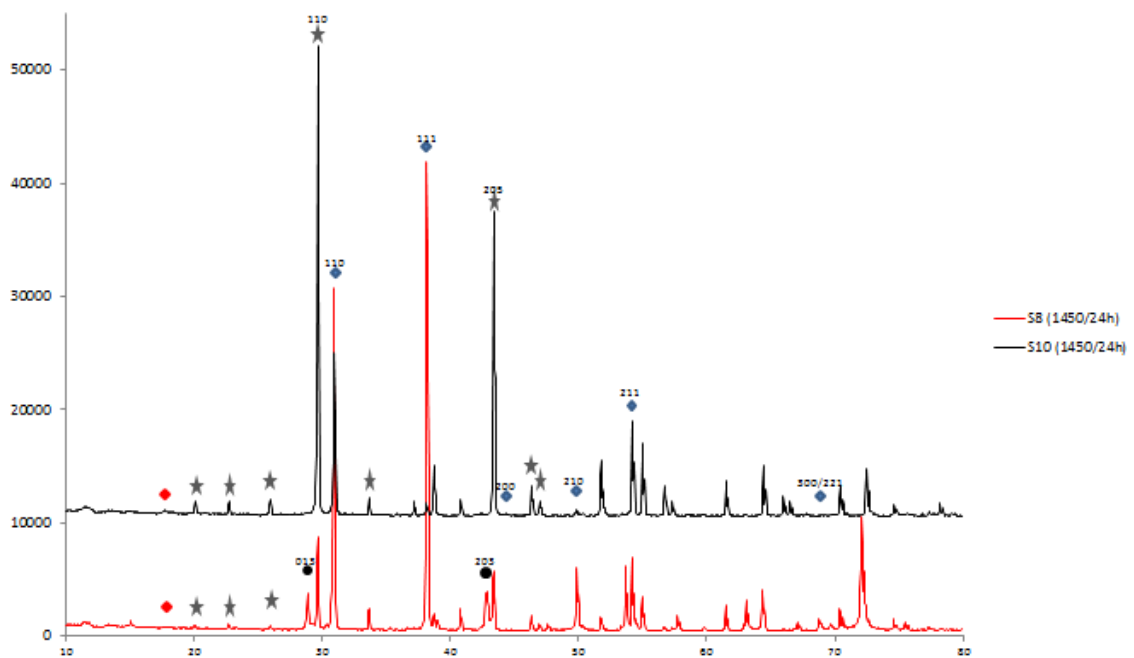


Fig. 4-23: XRD pattern of $\text{Ba}_3\text{Co}_{0.7}\text{Zn}_{0.3}\text{Nb}_2\text{O}_9$ series at various compositions. The samples were sintering at 1450°C for 24 hours (◆: superlattice, ◆: $\text{Ba}_3\text{Co}_{0.7}\text{Zn}_{0.3}\text{Nb}_2\text{O}_9$ (BCZN) phase, ★: $\text{Ba}_8(\text{Co},\text{Zn})_1\text{Nb}_6\text{O}_{24}$ phase, ●: $\text{Ba}_5\text{Nb}_4\text{O}_{15}$ phase).

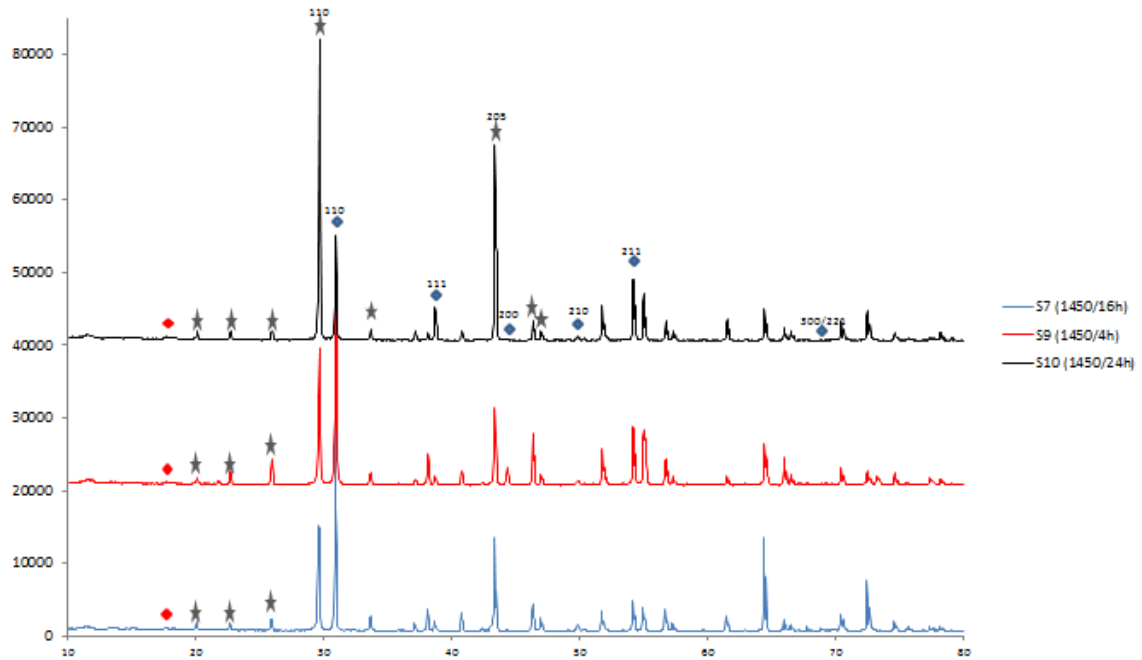


Fig. 4-24: XRD pattern of $\text{Ba}_3\text{Co}_{0.7}\text{Zn}_{0.3}\text{Nb}_2\text{O}_9$ series at various time, all sample sintering at 1450°C. (◆: superlattice♦: $\text{Ba}_3\text{Co}_{0.7}\text{Zn}_{0.3}\text{Nb}_2\text{O}_9$ (BCZN) phase★: $\text{Ba}_8(\text{Co},\text{Zn})_1\text{Nb}_6\text{O}_{24}$ phase●: $\text{Ba}_5\text{Nb}_4\text{O}_{15}$ phase).

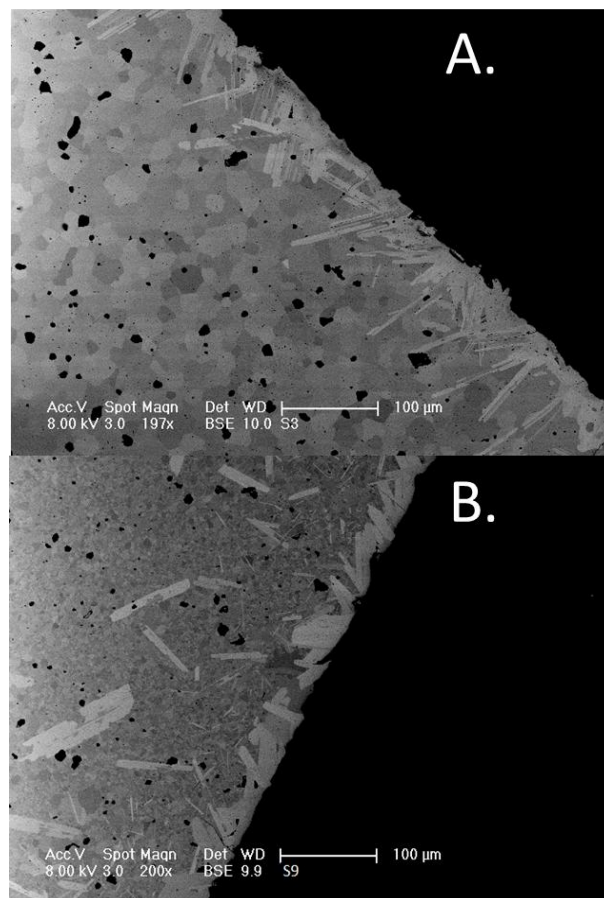


Fig. 4-25 SEM photographs of specimens with different composition sintered at 1450 °C/4 h.

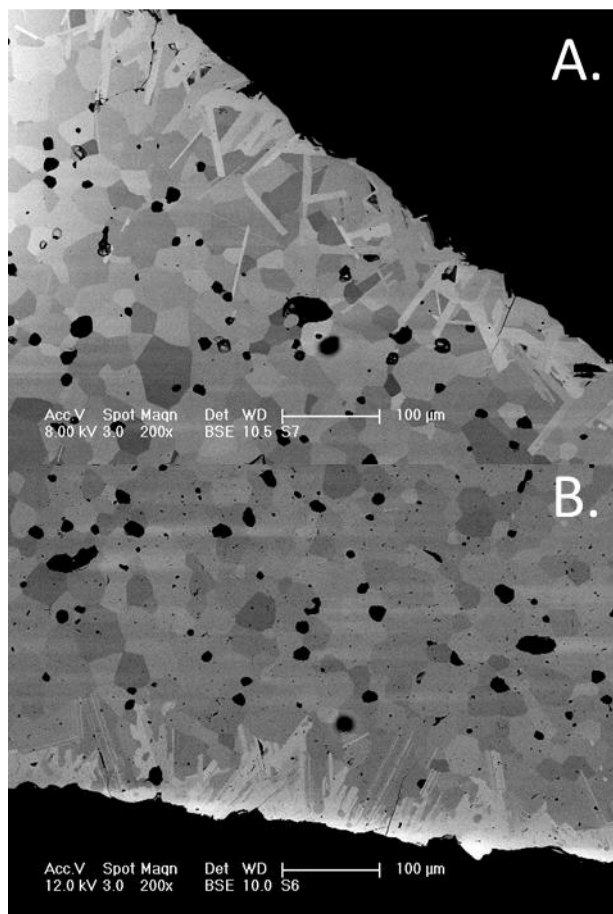


Fig. 4-26 SEM photographs of specimens with different composition sintered at 1450 °C/16 h.

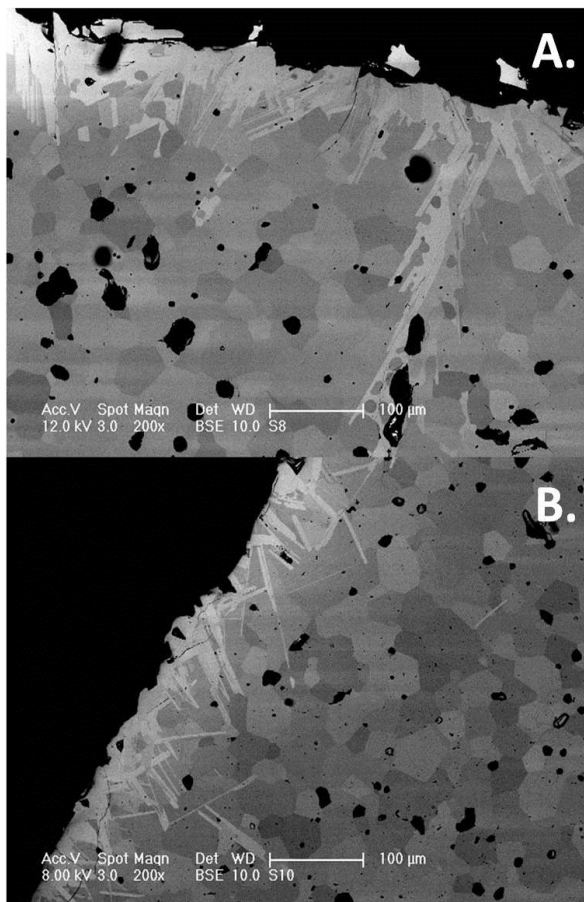


Fig. 4-27 SEM photographs of specimens with different composition sintered at 1450 °C/24 h.

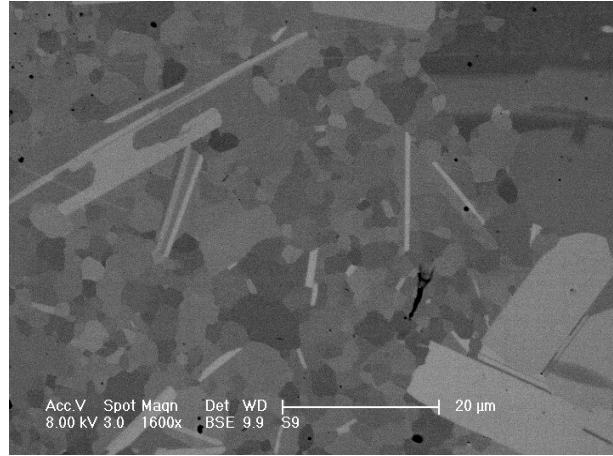


Fig. 4-28 SEM photographs of specimens sintering at 1450 °C/4 h closed to surface phase.

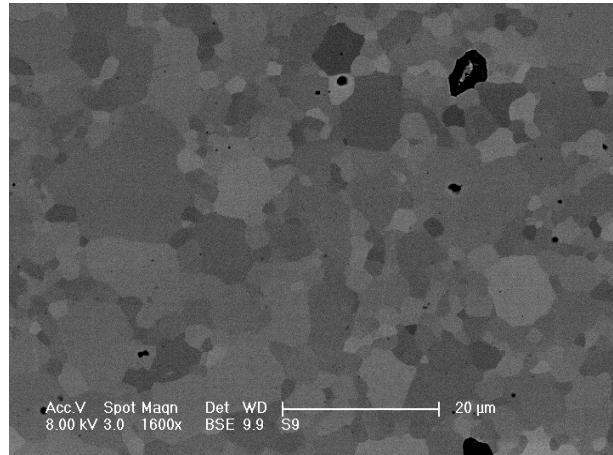


Fig. 4-29 SEM photographs of specimens sintering at 1450 °C/4 h closed to matrix phase.

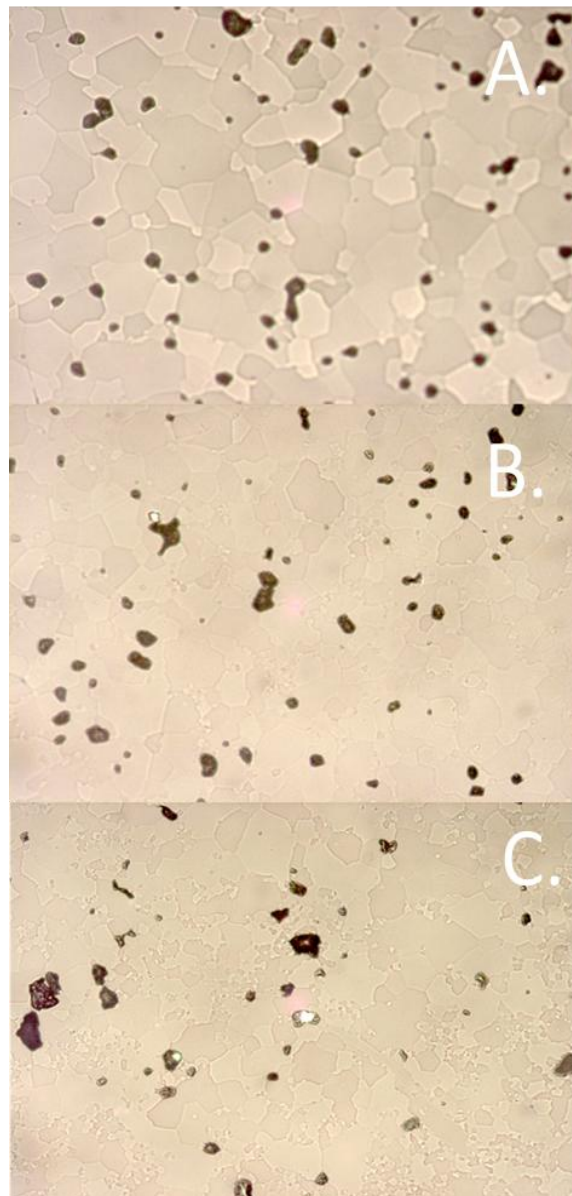


Fig. 4-30 Optical microscopy photographs of S10.

4.5 Overall discussion

In the above section, the result were shown and compared by different processing condition, therefore, this section attempt to identify the relationship between various conditions and microstructure, as well as Qxf value.

4.5.1 Comprehensive discussion of grain size

First, from the result shown as above, the main factor effect to grain size might be result from sintering time. In the above comparisons, the grain size only had slight change with thickness and volume changes; however, its variation can be seen clearly

when the sintering time change. This result can be confirmed by the past experiment which had been done by AHN et al [40, 41]. They set two experimental about BCN and (1-x)BCN-xBZN dielectric ceramics which were similar materials as this project used. The trend of grain growth was increased with the sintering go up. Therefore, the grain size and the amount of liquid phase have a close relationship. However, there was dramatically change in grain size due to composition change. S7, S9 and S10 have similar composition with varied sintering time and volume, sintering time not the only reason effect to grain size. Although the grain size in the edge similar trend as other sample, in the middle to substrate areas did not follow this trend. The result clearly indicated the grain size in S7 was bigger than it in S10, due to there are many small grain emerge in S10. This appearance might arise from thermal processing. In the past study, AHN et al [41] believed the increase in Qxf value with sintering time could be explained by the increase in grain size, however, this argument did not stand in this project, in which S1 and S6 occupied the top two of the ranking of Qxf value, but the grain size were much smaller than S8 which was sixth.

4.5.2 Comprehensive discussion of Qxf value

According to the result shown, as long as condition change, Qxf value would be changed, especially in sintering time and thickness changes. These two variables can be regarded as effect of thermal processing impact on materials. Hence, the changes of secondary phase, ordering parameter and domain size with different sintering schedule will be discussed in the following section, respectively:

4.5.2.1 Secondary phase

In all samples, secondary phase present in both XRD and SEM result; $\text{Ba}_8(\text{Co},\text{Zn})_1\text{Nb}_6\text{O}_{24}$ and $\text{Ba}_5\text{Nb}_4\text{O}_{15}$. The loss of Cobalt and Zinc might result in generation those secondary phase, in which $\text{Ba}_8(\text{Co},\text{Zn})_1\text{Nb}_6\text{O}_{24}$ is new type of complex perovsite [35] and has similar as $\text{Ba}_8\text{Ni}_1\text{Nb}_6\text{O}_{24}$ [42] and $\text{Ba}_8\text{Zn}_1\text{Nb}_6\text{O}_{24}$ [43], and $\text{Ba}_5\text{Nb}_4\text{O}_{15}$ contain excellent microwave dielectric properties of permittivity = $41 \text{ Q} \times f = 57000 \text{ GHz}$ and temperature coefficient= +78 ppm/ $^{\circ}\text{C}$ [44]. As the result shown from XRD, there is no enough evidence proof $\text{Ba}_5\text{Nb}_4\text{O}_{15}$ phase have great effect to Qxf value, due to it did not have

a great change. However, $\text{Ba}_8(\text{Co},\text{Zn})_1\text{Nb}_6\text{O}_{24}$ phase seems had bad influence to Qxf factor, due to relative intensity of $\text{Ba}_8(\text{Co},\text{Zn})_1\text{Nb}_6\text{O}_{24}$ phase tend increase as long as Qxf decrease. At the same time, there are more needle-shaped phase can be observed on SEM micrograph when Qxf value decrease. Therefore, the reason why Qxf value could be improved by increasing sintering time or reducing thickness might be arise from more cobalt and zinc evaporated or $\text{Ba}_8(\text{Co},\text{Zn})_1\text{Nb}_6\text{O}_{24}$ phase melted.

4.5.2.2 Ordering degree

Ordering parameter(S) [45, 46] is used to describe the cation ratio at B-site in complex perovskites structure system, and the value is 0 (completely disordering structure) and 1 (completely ordering structure). It can be determined by the ratio between superlattice peak and main peak [45, 47]. According to Warren [48] and Cullity [49] explained, the ordering parameter could be obtained. However, in this project, the author was using BCN system materials to derive the ordering parameter. All the works showed as below:

$$S = N_{\text{Nb}} - N_{\text{Co}} = C_{\text{Co}} - C_{\text{Nb}} \quad (4-1)$$

In which:

N_{Nb} : Fraction of niobium in Nb-sites.

N_{Co} : Fraction of Cobalt in Nb-sites.

C_{Co} : Fraction of Cobalt in Co-sites.

C_{Nb} : Fraction of niobium in Co-sites.

Then, calculate the intensity of Muller index:

$$I_{\text{hkl}} = kF_{\text{hkl}}^2MLp \quad (4-2)$$

In which:

k: Constant

F: Structure factor

M: Multiplicity factor

Lp: Lorentz-polarization factor

Then, the F_{hkl} in BCN system can be obtained as below:

$$\begin{aligned} F_{\text{hkl}} = & \sum f_0 \exp[2\pi i(hx_i + ky_i + lz_i)] \\ & + \sum f_{Ba} \exp[2\pi i(hx_i + ky_i + lz_i)] \\ & + \sum (C_{co}f_{co} + N_{co}f_{Nb}) \exp[2\pi i(hx_i + ky_i + lz_i)] \\ & + \sum (C_{Nb}f_{co} + N_{Nb}f_{Nb}) \exp[2\pi i(hx_i + ky_i + lz_i)] \end{aligned} \quad (4-3)$$

In which:

f : Scattering factor

Because of (100) is the superlattice reflection, and the strongest peak is (110). Otherwise (012) peak has similar intensity as (110), and (012) and (102) were overlapping peak, therefore put (100), (110), (012) and (102) into equation (4-3) and (4-1), the equation can be rewritten as below:

$$\begin{aligned} F_{110} &= 3f_{Ba} - 3f_O + (C_{Co} + 2C_{Nb})f_{Co} + (N_{Co} + 2N_{Nb})f_{Nb} \\ &= 3f_{Ba} - 3f_O + f_{Co} + 2f_{Nb} \end{aligned} \quad (4-4)$$

$$F_{102} = (C_{Co} - C_{Nb})f_{Co} - (N_{Co} + N_{Nb})f_{Nb} = (f_{Co} - f_{Nb})S \quad (4-5)$$

$$\begin{aligned} F_{110} &= 3f_{Ba} - 3f_O + (C_{Co} + 2C_{Nb})f_{Co} + (N_{Co} + 2N_{Nb})f_{Nb} \\ &= 3f_{Ba} - 3f_O + f_{Co} + 2f_{Nb} \end{aligned} \quad (4-6)$$

$$F_{102} = (C_{Co} - C_{Nb})f_{Co} - (N_{Co} + N_{Nb})f_{Nb} = (f_{Co} - f_{Nb})S \quad (4-7)$$

Due to scattering factor, multiplicity factor and Lorentz-polarization factors can found by Cullity's book [49], thus, the ordering parameter can be measured as following equation:

$$S^2 = \frac{654.202 \times I_{100}}{[4.296 \times (I_{100} + I_{120} + I_{012}) - I_{100}]} \quad (4-8)$$

From the equation 4-8, it is very clearly to prove why it is very difficult to observe superlattice peak in XRD result, due to the theoretical ratio of fully ordered structure should be 0.656%(when S=1). By using equation 4-8, the calculations show in Table 4-1. However, due to BCN system and BCZN system were not totally the same, all the date shown as Table 4-1 were Comparison value. Except S6 and S7 which have small volume, the date show ordering parameter might go up with sintering time increase or thickness reduce, meanwhile Qxf value increase. In the past study, Lee et al [50] attempted to use different sintering condition in BZN system, and try to figure the relationship between sintering condition and ordering parameter, as well as Qxf value. The results of this project have similar trend as Lee et al [50] study. Therefore, Qxf value could be improved by sintering condition, due to it might get higher ordering

parameter.

Table 4-1 Variation of ordering parameter

| S1 1450/4h OD:35.4m m Ht:4.82m m Qxf= 99976 | S2 1450/4h OD:35.6m m Ht:10.9m m Qxf= 22973 | S3 1450/4h OD:35.5m m Ht:14mm m Qxf= 12119 | S4 1450/12h OD:35.5m m Ht:14.1m m Qxf= 15517 | S5 1450/16h OD:35.5m m Ht:14.1m m Qxf= 65587 | S6 1450/16h OD:17mm Ht:6.95m m Qxf= 81431 | S7 1450/16h OD:17mm Ht:6.97m m Qxf= 75937 | S8 1450/24h OD:35.6m m Ht:14.0m m Qxf= 80651 | S9 1450/4h OD:35.5m m Ht:13.9m m Qxf= 77660 | S10 1450/24h OD:35.5mm Ht:14.0mm Qxf= 68880 |
|---|---|--|--|--|--|--|--|---|---|
| 0.84 | 0.70 | 0.55 | 0.63 | 0.73 | 0.61 | 0.68 | 0.66 | 0.67 | 0.66 |
| EDGE | | | | | | | | | |
| 0.77 | 0.76 | 0.63 | 0.72 | 0.77 | 0.58 | 0.65 | 0.56 | 0.71 | 0.70 |
| MIDDLE | | | | | | | | | |
| 0.67 | 0.64 | 0.68 | 0.79 | 0.77 | 0.60 | 0.68 | 0.64 | 0.66 | 0.81 |
| SUBSTRATE | | | | | | | | | |
| 0.76 | 0.70 | 0.62 | 0.71 | 0.76 | 0.59 | 0.67 | 0.62 | 0.68 | 0.73 |
| Avg | | | | | | | | | |

4.5.2.3 Domain size

Assuming there is no strain and faulting in the system, and then the main factor impact to the width of diffraction peak is domain size. The domain size can be calculated by scherrer formula which shows as below:

$$L = \frac{(0.9\lambda)}{FWHM \times \cos\theta_0} \quad (4-9)$$

In which:

L : Crystalline domain size (nm).

λ : Incident wavelength (nm).

$FWHM$: Full Width Half Maximum (Radian).

θ_0 : Diffraction angle (degree).

Table 4-2 shows the result of calculation domain size; all the works were using the same diffraction peak which was (110). In this project, except S6 and S7, the increase of domain size was increased with the sintering increased and thickness reduced. And compared with Qxf value, Qxf value tends to rise with domain size. According to Lee et al [51] study pointed out the energy loss might appear around domain boundary. Therefore, greater domain size might lead higher Qxf value, due to bigger domain size

can produce less domain boundary. Thus, Qxf value could be adjusted with various conditions; due to the domain size might different in different thermal processing. In addition, the trend of ordering parameter was similar as domain size.

Table 4-2 Variation of domain size

| | S1 1450/4h OD:35.4m m Ht:4.82m Qxf= 99976 | S2 1450/4h OD:35.6m m Ht:10.9m Qxf= 22973 | S3 1450/4h OD:35.5 mm Ht:14mm Qxf= 12119 | S4 1450/12h OD:35.5m m Ht:14.1m Qxf= 15517 | S5 1450/16h OD:35.5m m Ht:14.1m Qxf= 65587 | S6 1450/16h OD:17mm m Ht:6.95m Qxf= 81431 | S7 1450/16h OD:17mm m Ht:6.97m Qxf= 75937 | S8 1450/24h OD:35.6m m Ht:14.0m Qxf= 80651 | S9 1450/4h OD:35.5m m Ht:13.9m Qxf= 77660 | S10 1450/24h OD:35.5m m Ht:14.0mm Qxf= 68880 |
|-----------|--|--|---|---|---|--|--|---|--|---|
| EDGE | 44.67 | 40.95 | 40.94 | 42.96 | 44.82 | 40.95 | 35.09 | 46.72 | 37.80 | 46.81 |
| MIDDLE | 44.67 | 39.31 | 39.31 | 41.32 | 43.03 | 33.90 | 35.10 | 46.80 | 37.79 | 42.73 |
| SUBSTRATE | 44.67 | 44.67 | 40.95 | 41.32 | 43.04 | 36.41 | 36.39 | 44.68 | 36.40 | 39.31 |
| Avg | 44.67 | 41.64 | 40.40 | 41.87 | 43.63 | 37.09 | 35.53 | 46.06 | 37.33 | 42.95 |

Chapter V

CONCLUSION AND FUTURE WORK

5.1 Conclusion

This project reports research results about the BCZN series microwave dielectric materials with different processing condition, including height, sintering time, volume and composition. The main target of this study is to explore the relationship between processing condition and Q_{xf} value. Hence, several conclusions are summarized as follows:

1. BCZN series ceramic can achieve 95% theoretical density with sintering at 1450°.
2. No matter any processing condition, all sample revealed there are secondary phase formation.
3. BN phase were disappear when composition change, and there is no enough evidence show the BN phase has negative influence to the Q_{xf} value of BCZN series ceramics.
4. The grain size would be growth by increasing sintering time, in which the grain size reach the maxima when sintering at 1450°C for 24 hours in this project.
5. In XRD result show: In sample 1, 6, 7 and 9, the maxima Intensity belong to BCZN phase at 30.96 ° ; in sample 2, 4, 5 and 8 the maxima intensity belong to BCZN phase at 38.06 ° ; in sample 3 the maxima peak appear around 43 ° belong to 816 phase, finally, the sample 10 has a maxima peak around 29.6 ° belong to 816 phase. To compare with ranking of Q_{xf} value, the result demonstrated the main peak tend appear in BCZN phase at $2\theta=30.96^\circ$ when specimen has a higher Q_{xf} value, on the other hand, most of low Q_{xf} value specimens have a main peak belong to 816 phase. Therefore, 816 phase seems have negative effect to Q_{xf} value.
6. Q_{xf} value can be improved effectively by reducing height and increasing sintering

- time.
7. Qxf value can be effectively improved under the same condition which sintering 1450°C for 4 hours by changing composition, but tend to decrease when sintering time increase.
 8. BCZN series ceramic can obtain optimism Qxf value about 99976GHz, when materials sintering at 1450°C for 4 hours.
 9. Basically, Qxf value might increase with the domain size increase or ordering parameter close to 1.

5-2 Limitation

1. There is no information about annealing time and cooling rate.
2. The fully ordering parameter between BCN and BCZN are different.
3. There are two XRD machine been used, error may be relatively large.
4. The thickness of sample are different, therefore, it is difficult to choose the same area (XRD).

5-3 Future work

1. Making a model to solve the fully ordering parameter in complex perovskite structure system ($A(B_1B_2')B''O_3$).
2. In this project, S6 and S7 which have higher Qxf value contain lower ordering parameter and domain size. Try to investigate the reason.
3. Measuring the volume of each phase.
4. In order to figure out transition temperature between order- disorder phases, it is necessary to using varied temperature.

Reference

- [1] Richtmyer, R. D.; , "Dielectric Resonators," Journal of Applied Physics , vol.10, no.6, pp.391-398, Jun 1939.
- [2] Hughes, H.; Iddles, D. M.; Reaney, I. M.; , "Niobate-based microwave dielectrics suitable for third generation mobile phone base stations," Applied Physics Letters , vol.79, no.18, pp.2952-2954, Oct 2001.
- [3] Cohn, S.B.; , "Microwave Bandpass Filters Containing High-Q Dielectric Resonators," Microwave Theory and Techniques, IEEE Transactions on , vol.16, no.4, pp. 218- 227, Apr 1968.
- [4] S. Nomura, K. Toyama, and K. Kaneta, "Ba(Mg_{1/3}Ta_{2/3})O₃ Ceramics with Temperature-Stable High Dielectrics Constant and Low Microwave Loss," Japanese Journal Applied Physics, 21, pp.624-626 1982.
- [5] H. Ohsato, T. Tsunooka, A. Kan, Y. Ohishi, Y. Miyauchi,Y. Tohdo, T. Okawa, K. Kakimoto, and H. Ogawa, "Microwave-Millimeterwave Dielectric Materials," Key Engineering Materials, 269, pp.195-198 2004.
- [6] R. Freer, F. Azough, "Microstructural engineering of microwave dielectric ceramics," Journal of the European Ceramic Society 28 1433–1441 2008.
- [7] O.Prytz and J.Tafto, "Accurate Determination of Orientation Relationships between Ferroelastic Domains : The Tetragonal to Monoclinic Transition in LaNbO₄ as an example," Acta Mat., 53,297-302 2005.
- [8] W. D. Kingery, H. K. Bowen, and D. R. Uhlmann, Introduction to Ceramics, 2nd Ed., 92 John Wiley and Sons, New York 1976.
- [9] H. ouchi and S. Kawashima, "Dielectric Ceramics for Microwave Application," Jpn. J. Appl. Phys., 24 [suppl. 24-2], 60-64 (1985).
- [10]. 吳朗，電子陶瓷，全欣科技圖書 (1994)。
- [11]2-5. K. Wakine, "Recent Development of Dielectric Resonator Materials and Filters in Japan," Ferroelectrics, 91, pp. 69-86 1989.
- [12] W. Wersing, High Frequency Ceramic Dielectrics and their Application for Microwave, in Electronic Ceramics, edited by B. C. H. Steele, 67 1991.
- [13] F. V. Lenel, "Sintering in Presence of a Liquid Phase," Trans. Am.Inst. Mining Met. Engrs, pp.878-905, 1948.

- [14] David K. Cheng, "Field and Wave Electromagnetics" 2th edition, Addison Wesley, New York pp 406-410, 407-412 1989.
- [15]. L. L. Hench and L. K. West, "Principles of Electronic Ceramics", (John Wiley & Sons, Inc.), pp244-247, 1990.
- [16] P.K. Davies, H.Wu, A.Y. Borisevich, I.E. Molodetsky, and L. Farber5, "Crystal Chemistry of Complex Perovskites: New Cation-Ordered Dielectric Oxides", Annu. Rev. Mater. Res. 38:369–401 2008.
- [17] A. S. Bhalla, Ruyan Guo, and Rustum Roy, "The Perovskite Structure – a Review of its Role in Ceramic Science and Technology," Mat. Res. Innovat., 4, 3–26, 2000.
- [18] Randall M. German, "Liquid Phase Sintering," Plenum Press, New York 1985.
- [19] W. J. Huppmann and G. Petzow, "The Elementary Mechanisms of Liquid Sintering, Sintering Processes," Edited by G. C. Kuczynski, New York: Plenum Press, 189-202 1979.
- [20] W. D. Kingery, "Densification During Sintering in Presence of a Liquid Phase", J. Appl. Phys. vol.3, pp.301-306, 1959.
- [21] R. B. Heady and J. W. Cahn, "An Analysis of the Capillary Forces in Liquid-Phase Sintering of Spherical Particles", Metall. Trans. vol.1, pp.185-189, 1970.
- [22] R. C. Kell, A. C. Grenham, and G. C. E. Olds, "High Permittivity Temperature-Stable Ceramic Dielectric with Low Microwave Loss," Journal of the American Ceramic Society, 56, pp.352-354 1973.
- [23] T. Yamaguchi, Y. Komatsu, T. Otobe, and Y. Murakami, "Newly Developed Ternary (Ca,Sr,Ba) Zirconate Ceramic System for Microwave Resonator," Ferroelectrics, 27, pp.273-276 1980.
- [24] S. Nomura, K. Toyama, and K. Kaneta, "Ba (Mg_{1/3}Ta_{2/3})O₃ Ceramics with Temperature-Stable High Dielectrics Constant and Low Microwave Loss," Jpn. J. Appl. Phys. 21 pp. L624-L626 1982.
- [25] P. C. Osbond, R. W. Whatmore, and F. W. Ainger, "The Properties and Microwave Application of Zirconium Titanate Stannate Ceramics," British Ceramic Proceedings, 36, pp.167-168 1985.
- [26] K. Wakino, K. Minai, and H. Tamura, "Microwave Characteristics of (Zr_xSn_y)TiO₄ and BaO-PbO-Nd₂O₃-TiO₂ Dielectric Resonators," Journal of the American Ceramic Society, 67, pp.278-281 1984.

- [27] H. M. O'Bryan, and J. Thomson. JR, "Phase Equilibrium in the TiO₂-rich Region of the System BaO-TiO₂," *Journal of the American Ceramic Society*, 57, pp.522-526 1974.
- [28] H. M. O'Bryan, J. Thomson. JR, and J. K. Plourde, "A New BaO-TiO₂ Compound with Temperature-stable High Permittivity and Low Microwave Loss," *Journal of the American Ceramic Society*, 57, pp.450-453 1974.
- [29] S. Kawashima, I. Nishida, I. Ueda, and H. Ouchi, "Dielectric Properties of Ba (Zn_{1/3}Nb_{2/3})O₃-Ba (Zn_{1/3}Ta_{2/3})O₃ Ceramics," *American Ceramic Society Bulletin*, 60, pp.401 1981.
- [30] H. Hughes, F. Azougha, R. Freer, D. Iddles, "Development of surface phases in Ba (Zn_{1/3}Nb_{2/3})O₃-Ba (Ga_{1/2}Ta_{1/2})O₃ microwave dielectric ceramics", *Journal of the European Ceramic Society* 25 2755–2758 2005.
- [31] Azough, C. Leach, R. Freer, "Effect of nonstoichiometry on the structure and microwave dielectric properties of Ba (Co_{1/3}Nb_{2/3})O₃ ceramics". *Journal of the European Ceramic Society* 26 2877–2884 2006.
- [32] Cheol-Woo Ahn, Hyun-Jung Jang, Sahn Nahm, Hyun-Min Park, Hwack-Joo Lee, "Effects of microstructure on the microwave dielectric properties of Ba (Co_{1/3}Nb_{2/3})O₃ and (1-x)Ba (Co_{1/3}Nb_{2/3})O₃-xBa (Zn_{1/3}Nb_{2/3})O₃ ceramics", *Journal of the European Ceramic Society* 23 2473–2478 2003.
- [33] KAZUAKI ANDO, K ENJIF UJIMOTO and KYOHEIM URAKAWA, "Dielectric Properties of Ceramics in Ba (Co_{1/3}Nb_{2/3})O₃-Ba (Zn_{1/3}Nb_{2/3})O₃ solid Solutions", *Communications of the American Ceramic Society C-215*, *Communications of the American Ceramic Society. J. Am. Cerum. SOC.*, 70 [9] C-215-C-218 1987.
- [32] Cheol-Woo Ahn, Hyun-Jung Jang, Sahn Nahm, Hyun-Min Park, Hwack-Joo Lee, "Effects of microstructure on the microwave dielectric properties of Ba (Co_{1/3}Nb_{2/3})O₃ and (1-x)Ba (Co_{1/3}Nb_{2/3})O₃-xBa (Zn_{1/3}Nb_{2/3})O₃ ceramics", *Journal of the European Ceramic Society* 23 2473–2478 2003.
- [34] F. Azough, C. Leach, and R. Freer, "Niobate Complex Perovskite Microwave Dielectric Ceramics Ba(Me_{1/3}Nb_{2/3})O₃ (Me= Zn, Co, Ni and Mg)", *Advances in Science and Technology* Vol. 45 pp 2323-2331 2006.
- [35] F. Azough, C. Leach, R. Freer, "Effect of CeO₂ on the sintering behaviour, cation

- order and properties of Ba₃Co0.7Zn0.3Nb₂O₉ ceramics,” Journal of the European Ceramic Society 26 1883–1887 2006.
- [36] M. Barwick, F. Azough, R. Freer, “Structure and dielectric properties of perovskite ceramics in the system Ba (Ni₁/3Nb₂/3)O₃–Ba (Zn₁/3Nb₂/3)O₃”, Journal of the European Ceramic Society 26 1767–1773 2003.
- [37] F. Azough, C. Leach, R. Freer, “Effect of V₂O₅ on the sintering behaviour, cation order and properties of Ba₃Co0.7Zn0.3Nb₂O₉ ceramics”, Journal of the European Ceramic Society 25 2839–2841 2005.
- [38] H. Hughes, F. Azougha, R. Freer, D. Iddles, “Development of surface phases in Ba (Zn₁/3Nb₂/3)O₃–Ba (Ga₁/2Ta₁/2)O₃ microwave dielectric ceramics”, Journal of the European Ceramic Society 25 2755–2758 2005.
- [39] Ki Hyun Yoon, Dong Pil Kim, and Eung Soo Kim, “Effect of BaWO₄ on the microwave dielectric properties of Ba(Mg₁/3Ta₂/3)O₃ ceramics,” J. Am. Ceram. Soc., 77[4] p.1062-66 1994.
- [40] Cheol-Woo AHN, Sahn NAHM, Yun-Soo LIM, Woong CHOI, Hyun-Min PARK and Hwack-Joo LEE, “Microstructure and Microwave Dielectric Properties of Ba(Co₁/3Nb₂/3)O₃ Ceramics” , Jpn. J. Appl. Phys. Vol. 41 pp. 5277 – 5280, Part 1, No. 8, August 2002.
- [41] Cheol-Woo AHN, Sahn NAHM, Yun-Soo LIM, Woong CHOI, Hyun-Min PARK and Hwack-Joo LEE, “Microstructure and Microwave Dielectric Properties of (1-x)Ba(Co₁/3Nb₂/3)O₃ – xBa(Zn₁/3Nb₂/3)O₃ Ceramics”, Jpn. J. Appl. Phys. Vol. 42 pp. 6964 – 6968 Part 1, No. 11, November 2003.
- [42] Abakumov, A. M., Tendeloo, G. V., Scheglov, A. A., Shpanchenko, R. V. and Antipov, E. V., The crystal structure of Ba₈Ni₁Nb₆O₂₄: cation ordering in hexagonal perovskites. J. Solid State Chem., 125, 102–107 1996.
- [43] Azough, F. and Freer, R., The crystal structure and dielectric properties of Ba₈Zn₁Nb₆O₂₄ ceramics, unpublished.
- [44] Ratheesh, R. Sebastian, M. T. Mohanan, P. Tobar, M. E. Hartnett, J. Woode, R. et al., Microwave characterisation of BaCe₂Ti₅O₁₅ and Ba₅Nb₄O₁₅ ceramic dielectric resonators using whispering gallery mode method. Mater. Lett., 45(5),

279–285 2000.

- [45] Lu, C. H. and Tsai, C. C., “Reaction Kinetics, Sintering Characteristics, and Ordering Behavior of Microwave Dielectrics: Barium Magnesium Tantalite,” *J. Mater. Res.*, 11, 1219–1227 1996.
- [46] Matsumoto, K., Hiuga, T., Takada, K. and Ichimura, H., Ba(Mg_{1/3}Ta_{2/3})O₃ ceramics with ultra-low loss at microwave-frequencies. In Proceedings of the 6th IEEE International Symposium on the Applications of Ferroelectrics, IEEE, New York, , p. 118 2000.
- [47] I. M. Reaney, Y. Iqbal, H. Zheng, A. Feteira, H. Hughes, D. Iddles, D. Muir, T. Price, “Order–disorder behaviour in 0.9Ba([Zn0.60Co0.40]1/3Nb_{2/3})O₃–0.1Ba(Ga0.5Ta0.5)O₃ microwave dielectric resonators”, *Journal of the European Ceramic Society* 25 1183–1189 2005.
- [48] Warren, B. E., X-Ray Diffraction. Dover Publication, New York, 1969.
- [49] Cullity, B. D., Elements of X-Ray Diffraction. Addison-Wesley Publishing, Reading, MA, 1978.
- [50] Chun-Te Lee, Yi-Chang Lin, Chi-Yuen Huang, Che-Yi Su, and Ching-Li Hu, “Cation Ordering and Dielectric Characteristics in Barium Zinc Niobate,” *J. Am. Ceram. Soc.*, 90 [2], 483-489 2007.
- [51] H. J. Lee, H. M. Park, Y. W. Song, Y. K. Cho, J. H. Paik, S. Nahm, and J. D. Byun, “Two Types of Domain Boundaries in Lanthanum Magnesium Niobate”, *J. Am. Ceram. Soc.*, 83 [11], 2875-2877 2000.